Lawrence Livermore National Laboratory

2014 LLNL Nuclear Forensics Summer Program

Glenn T. Seaborg Institute
Lawrence Livermore National Laboratory
Physical and Life Sciences Directorate
Livermore, CA 94550

Director: Annie Kersting (kersting1@llnl.gov)
Administrator: Camille Vandermeer
Website: https://seaborg.llnl.gov/

Sponsors:
National Technical Nuclear Forensics Center, Domestic Nuclear Detection Office, Department of Homeland Security
LLNL: Glenn T. Seaborg Institute, Physical and Life Sciences Directorate

Lawrence Livermore National Laboratory is operated by Lawrence Livermore National Security, LLC, for the U.S. Department of Energy, National Nuclear Security Administration under Contract DE-AC52-07NA27344.

LLNL-TR-664996

Disclaimer

Auspices

This work was performed under the auspices of the U.S. Department of Energy by Lawrence Livermore National Laboratory under Contract DE-AC52-07NA273

Figure 1. Annie Kersting, Director, Glenn T. Seaborg Institute (far left), and 2014 Nuclear Forensics Summer Program Students and Nuclear Forensics Graduate Fellows

The Lawrence Livermore National Laboratory (LLNL) Nuclear Forensics Summer Program is designed to give graduate students an opportunity to come to LLNL for 8–10 weeks for a hands-on research experience. Students conduct research under the supervision of a staff scientist, attend a weekly lecture series, interact with other students, and present their work in poster format at the end of the program. Students also have the opportunity to meet staff scientists one-on-one, participate in LLNL facility tours (e.g., the National Ignition Facility and Center for Accelerator Mass Spectrometry) to gain a better understanding of the multi-disciplinary, on going science at LLNL.

Currently called the Nuclear Forensics Summer Program, this program began 14 years ago as the Actinide Sciences Summer Program. The program is run within the Glenn T. Seaborg Institute in the Physical and Life Sciences Directorate at LLNL. The goal of the Nuclear Forensics Summer Program is to facilitate the training of the next generation of nuclear scientists and engineers to solve critical national security problems in the field of nuclear forensics and have the students participate in conducting research at LLNL. We select students who are majoring in physics, chemistry, geology, mathematics, nuclear engineering, chemical engineering and environmental sciences. Students engage in research projects in the disciplines of actinide chemistry, radiochemistry, isotopic analysis, computational analysis, radiation detection, and nuclear engineering in order to strengthen the "pipeline" for future scientific disciplines critical to DHS (DNDO), NNSA.

This is a competitive program with over 80 applicants for the 8–12 slots available. Students also come on paid internships from NNSA, DHS. Students come highly recommended from universities all over the country. For example, this year we hosted students from 11 different universities. (See Table 1). This year's students conducted research on such diverse topics as actinide (Np, U, Pu) isotopic fingerprinting, statistical modeling in nuclear forensics, environmental radiochemistry, heavy element separations chemistry, radiation detector physics development, nuclear chemistry, and scintillator materials development (see Table 2.) Graduate students are invited to return for a second year at their mentor's discretion. We encourage continuation of research collaboration between graduate student, faculty advisor, and LLNL scientists.

In addition to hands-on training, students attend a weekly lecture series on topics applicable to the field of nuclear forensics (see Table 3). Speakers are experts from both within LLNL and the national community. Speakers are able to discuss the importance of their work in the context of advances in the field of nuclear forensics.

Graduate and undergraduate students on fellowships such as the Nuclear Forensics Graduate Fellowship are invited into our summer program. They usually come for 12 weeks and can return the following summer or stay throughout the year depending on their research needs. This year we had 3 Nuclear Forensics Fellows, 2 in the graduate program and one in the undergraduate program (Table 1, noted by an asterisks).

We also host students who are participating in the DOE-sponsored "Summer School in Radiochemistry" course held at San Jose State University and have recruited from this program. They come for a day, meet our summer students, see the research our students are doing, and tour our facilities. Staff scientists also participate in the Nuclear Forensics Undergraduate Summer Program sponsored by DHS-DNDO (FY14 held at University of Missouri, MO). Staff scientists lecture to the undergraduate students in their field of expertise.

We use our summer program to help develop a successful pipeline of top-quality students from universities across the U.S. Since 2002, 30-40% have returned to conduct their graduate research at LLNL:

- 14 became postdoctoral fellows at LLNL.
- 6 became postdoctoral fellows at other national labs.
- 9 were hired as career scientists at LLNL.
- 3 were hired as career scientists at other national labs.
- 3 were hired as faculty in the area of nuclear forensics/radiochemistry/nuclear science.

A big factor in the success of this program is the dedication of the staff scientists who volunteer to mentor the summer students. In FY14, funding from the Nuclear Forensics Graduate Mentoring Program (sponsor: DNDO) helped to partially support the time staff took to teach the summer interns. Staff scientists were able to take the necessary time to develop an appropriate summer project for their student, oversee necessary safety training, and dedicate more time to helping the interns maximize their productivity and scientific potential.

The posters presented at our Laboratory Student Poster Day are included at the end of this report. Once again, one of our student's poster won the 'best poster' award out of about 250 students posters that were judged.

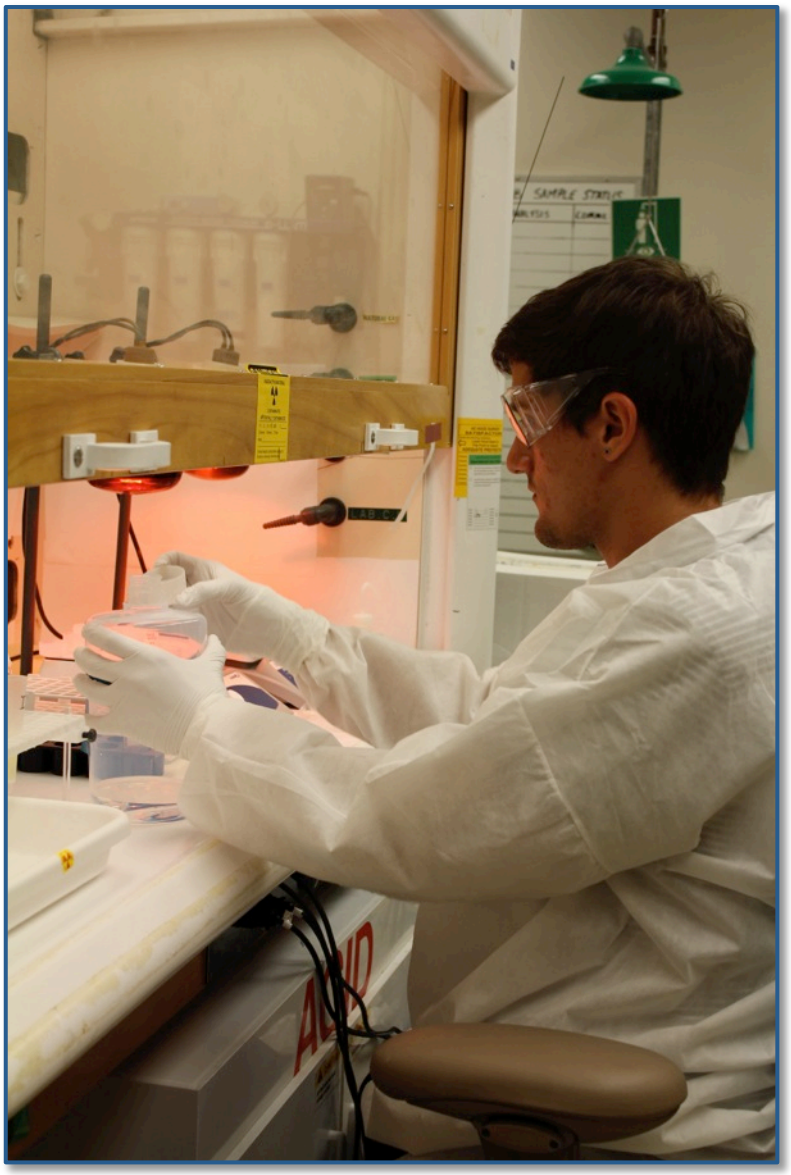

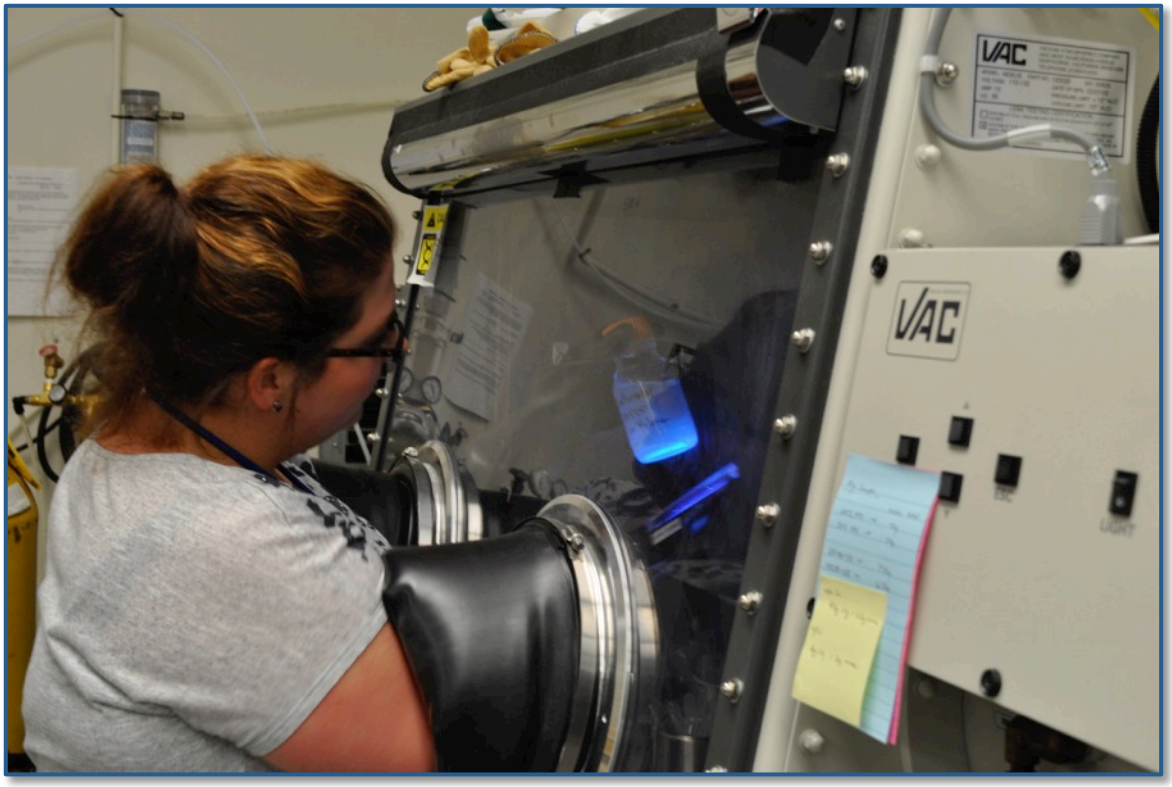
VAC
VAC


CAMECA
IMS 3F

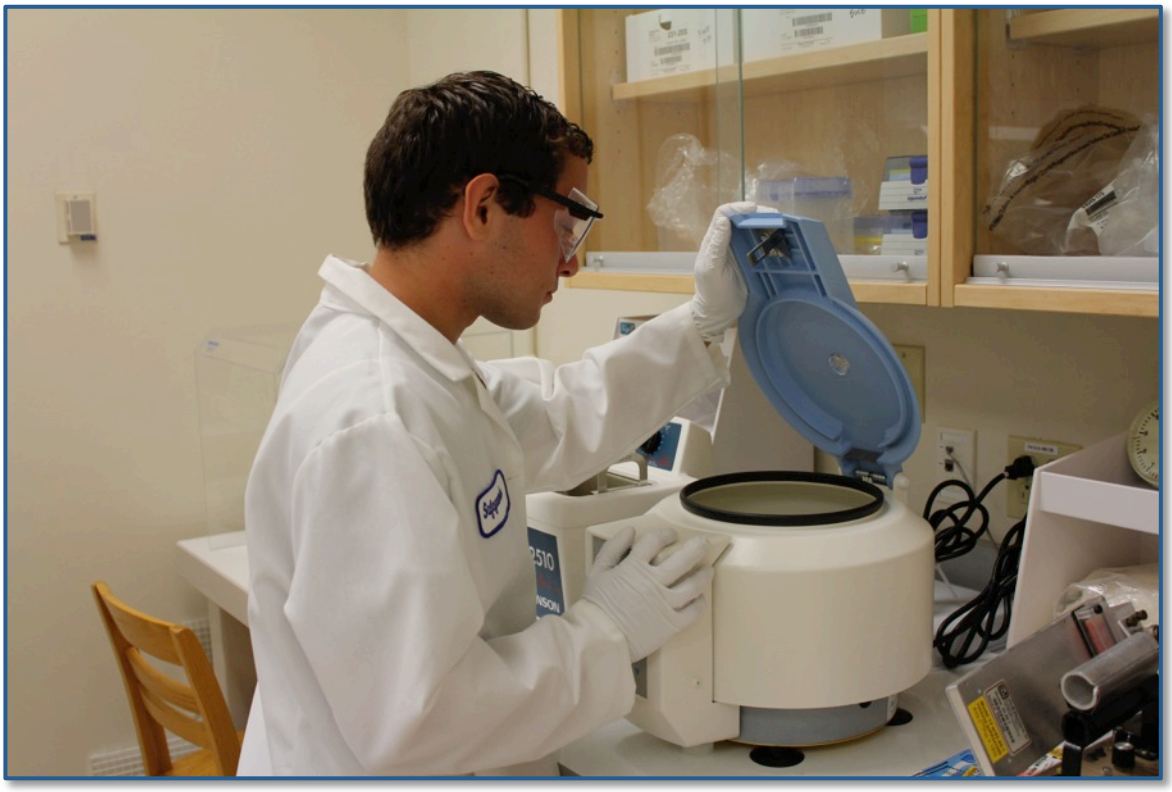

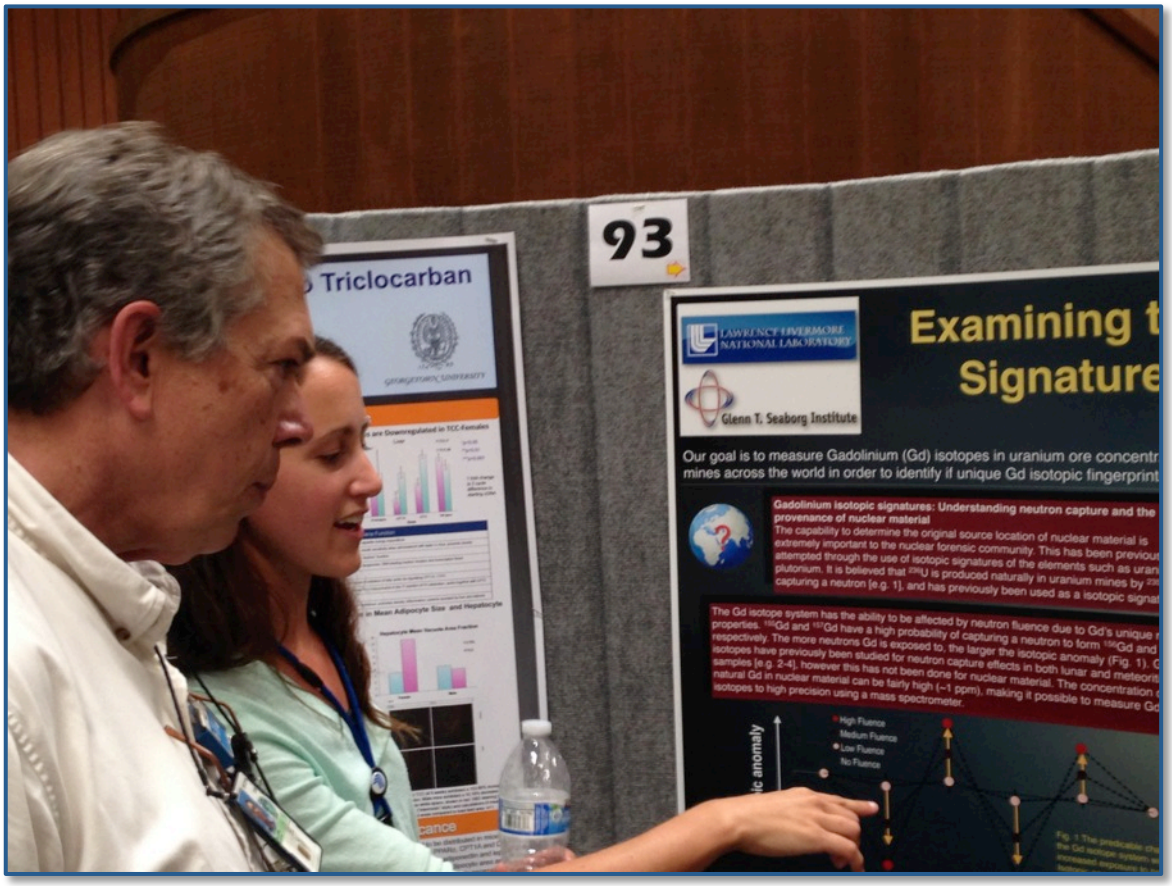
93
Triclocarban
Examining t
Signature
Glenn T. Seaborg Institute
Our goal is to measure Gadolinium (Gd) isotopes in uranium ore concentr
mines across the world in order to identify if unique Gd isotopic fingerprint
Gadolinium isotopic signatures: Understanding neutron capture and the
provenance of nuclear material
High Fluence
Medium Fluence
Low Fluence
No Fluence

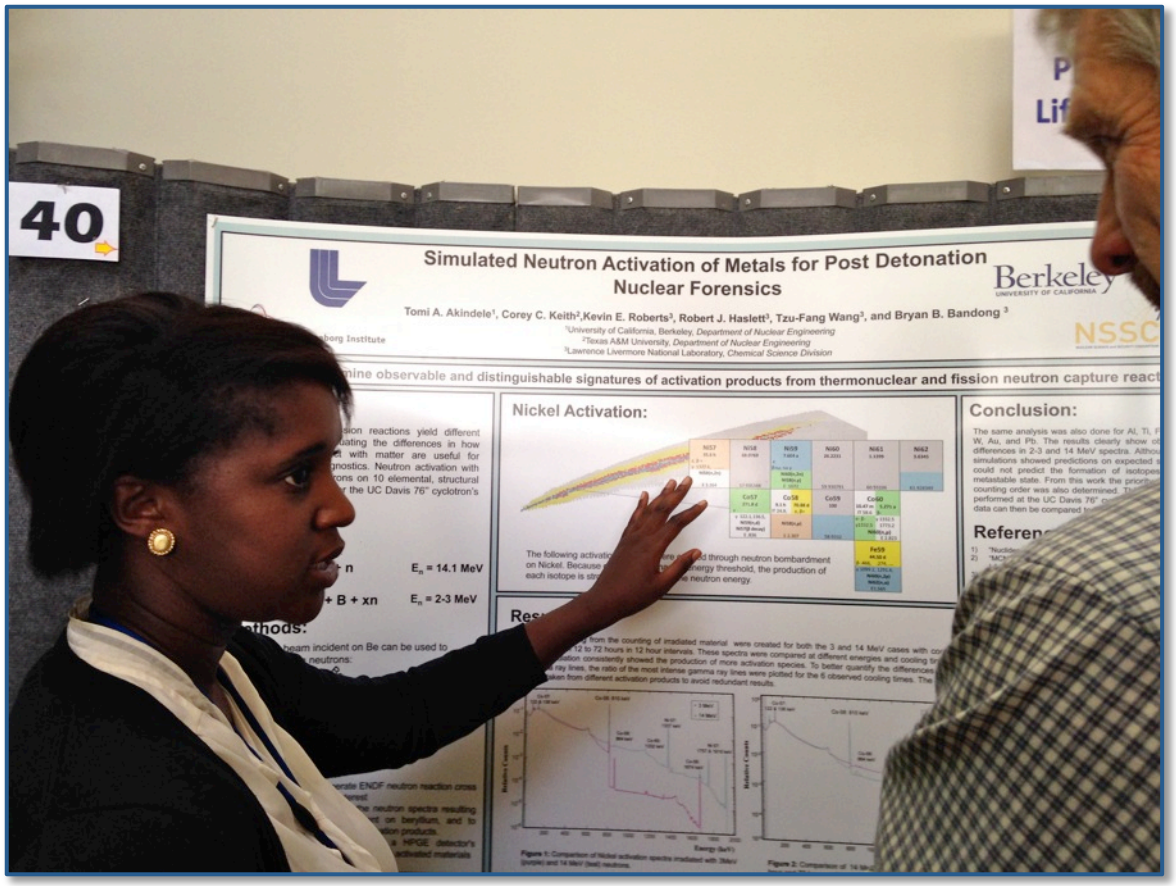
40
Simulated Neutron Activation of Metals for Post Detonation
Nuclear Forensics
Berkeley
Tomi A. Akindele[1], Corey C. Keith[2],Kevin E. Roberts[3], Robert J. Haslett[3], Tzu-Fang Wang[3], and Bryan B. Bandong [3]
[1]University of California, Berkeley, Department of Nuclear Engineering
[2]Texas A&M University, Department of Nuclear Engineering
[3]Lawrence Livermore National Laboratory, Chemical Science Division
Nickel Activation:
Conclusion:
E_n ≈ 14.1 MeV
E_n ≈ 2-3 MeV

Table 1. Summer Students

Student	Major	University	Year
Oluwatomi Akindele	Nuclear Engineering	University of California, Berkeley	Grad
Richard Beck	Nuclear and Radiological Engineering	Texas A&M University	Grad
Andrew Conant**	Nuclear and Radiological Engineering	George Institute of Technology	Undergrad
Kelly Daniel	Forensic Science	Marshall University	Grad
Megan Deeds	Chemistry	University of Cincinnati	Grad
Marc Fitzgerald*	Chemistry	University of Nevada, Las Vegas	Grad
Connor Hilton**	Geochemistry	Brown University	Undergrad
Corey Keith	Nuclear Engineering	Texas A&M University	Grad
Kelly Kmak**	Chemistry	University of California, Berkeley	Undergrad
Laurence Lewis	Nuclear Engineering	University of California, Berkeley	Grad
Chris Prokop	Nuclear Chemistry	Michigan State University	Grad
Andrew Renshaw	Geology	California State University, East Bay	Grad
Quinn Shollenberger**	Chemistry	Arizona State University	Undergrad
Rodrigo Tapia**	Mathematics and Chemistry	University of Georgia	Undergrad

*= Nuclear Forensics Graduate Fellows ** = Nuclear Forensics Undergraduate Intern

Table 2. Student Projects and Mentors

Student	Mentor	Project
Oluwatomi Akindele	Bryan Bandong, Kevin Roberts	Simulated Neutron Activation of Metals for Post Detonation Nuclear Forensics
Richard Beck	Nicholas Scielzo	β -Delayed α Angular Correlation in Mass 8 Systems
Andrew Conant	Martin Robel	Reactor Modeling of Pu and Cs Isotope Ratios in Pressurized Water Reactor Fuel Assemblies
Kelly Daniel	Mike Kristo	Evaluating Methods for Removing Radioactive Contamination from Traditional Forensic Evidence: Moths
Megan Deeds	Natalia Zaitzeva	Exploring Polymerization Techniques for PSD Plastic Scintillators
Marc Fitzgerald**	Kim Knight	Understanding Plutonium in Fallout Formation
Connor Hilton*	Ross Williams	Local and Global Nuclear Fallout Contributions to a Soil Profile
Corey Keith	Bryan Bandong, Kevin Roberts	High-Energy Neutron Foil Activation for Davis Cals
Kelly Kmak	Dawn Shaughnessy	Separations and Nuclear Counting for Research Projects on National Ignition Facility (NIF) Radiochemistry and Nuclear Forensics Sample Production
Laurence Lewis	Ian Hutcheon	SIMS Analysis of Aerodynamic Fallout
Chris Prokop	Dawn Shaughnessy	Perform Isotope Production and Nuclear Counting Experiments in Support of Nuclear Forensics
Andrew Renshaw	Brad Esser	Investigation of Radium Analytical Methods for Groundwater with Complex Matrices
Quinn Shollenberger	Greg Brennecka	Examining the Gadolinium Isotopic Signatures of Nuclear Material
Rodrigo Tapia**	Gary Eppich, Sarah Roberts	Comparison of Historical Fallout with Representative Soil Samples by XRD and ICP-MS

* = Nuclear Forensics Undergraduate Intern **= Nuclear Forensics Graduate Fellows

Table 3. Seminar Schedule

Date	Speaker	Topic
6/12/14	**Kim Knight** Staff Scientist, Chemical & Isotopic Signatures Group, Chemical Sciences Division	**Analytical Chemistry: Applications in Nuclear Forensics**
6/26/14	**James Begg** Staff Scientist, Environmental Radiochemistry Group, Chemical Sciences Division	**Water, Rocks and Microbes: The Biogeochemistry of Radionuclides**
7/1/14	**Dawn Shaughnessy** Group Leader, Experimental Nuclear and Radiochemistry, Chemical Sciences Division	**Radiochemistry and Nuclear Physics Measurements at the National Ignition Facility**
7/8/14	**Jean Moran** Associate Professor California State University East Bay, Department of Earth and Environmental Sciences	**Studying the Effects of Climate Change on Water Resources Using Isotopes**
7/16/14	**Amy Gaffney** Staff Scientist, Chemical & Isotopic Signatures Group, Chemical Sciences Division	**Chronometry of Geologic and Nuclear Materials**
	Brett Isselhardt Staff Scientist, Chemical & Isotopic Signatures Group, Chemical Sciences Division	**Resonance Ionization Mass Spectrometry Analysis for Nuclear Forensics**
7/24/14	**Mark Stoyer** Group Leader, Experimental Nuclear Physics, Physics Division	**Nuclear Forensics at LLNL**
7/31/14	**Mona Dreicer** Deputy Program Director for Nuclear and Domestic Security and Deputy Director of the Center for Global Security Research (CGSR)	**Treaty Monitoring and Verification**
8/8/14	**Annie Kersting** Director, Glenn T. Seaborg Institute, Physical and Life Sciences Directorate	**Closing out the Program**

Simulated Neutron Activation of Metals for Post Detonation Nuclear Forensics

Tomi A. Akindele[1], Corey C. Keith[2],Kevin E. Roberts[3], Robert J. Haslett[3], Tzu-Fang Wang[3], and Bryan B. Bandong [3]

[1]University of California, Berkeley, *Department of Nuclear Engineering*
[2]Texas A&M University, *Department of Nuclear Engineering*
[3]Lawrence Livermore National Laboratory, *Chemical Science Division*

Objective: Determine observable and distinguishable signatures of activation products from thermonuclear and fission neutron capture reactions

Introduction:

Thermonuclear and fission reactions yield different energy neutrons. Evaluating the differences in how these neutron interact with matter are useful for nuclear forensics diagnostics. Neutron activation with 2-3 and 14 MeV neutrons on 10 elemental, structural metals was simulated for the UC Davis 76'' cyclotron's deuteron beam.

Theory:

Thermonuclear reaction:

$^{2}H + {}^{3}H \rightarrow {}^{4}He + n$ $\quad E_n = 14.1$ MeV

Fission reaction:

$n + {}^{235}U \rightarrow A + B + xn$ $\quad E_n = 2\text{-}3$ MeV

Methods:

A deuteron beam incident on Be can be used to create spallation neutrons:

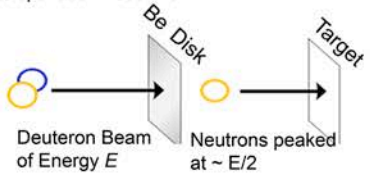

1) PYNE was used to generate ENDF neutron reaction cross sections for energies of interest
2) MCNP was used to model the neutron spectra resulting from a deuteron beam incident on beryllium, and to calculate the concentration of activation products.
3) GADRAS was used to simulate a HPGE detector's response to the gamma rays from the activated materials

Nickel Activation:

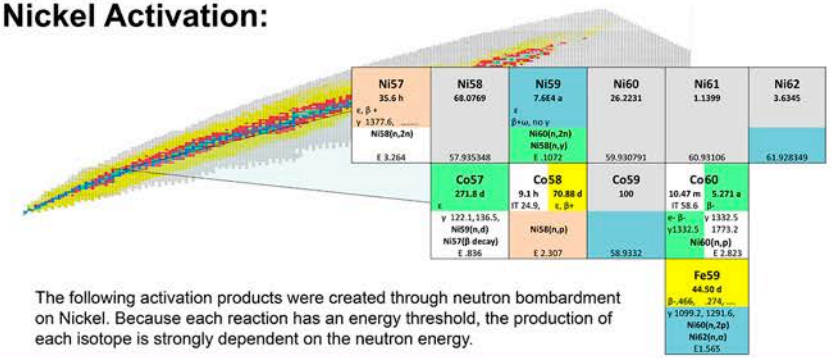

The following activation products were created through neutron bombardment on Nickel. Because each reaction has an energy threshold, the production of each isotope is strongly dependent on the neutron energy.

Conclusion:

The same analysis was also done for Al, Ti, Fe, Cu, Ir, W, Au, and Pb. The results clearly show observable differences in 2-3 and 14 MeV spectra. Although these simulations showed predictions on expected spectra, it could not predict the formation of isotopes in their metastable state. From this work the priority of sample counting order was also determined. This work is to be performed at the UC Davis 76'' cyclotron. Experimental data can then be compared to the simulated results.

References:

1) "Nuclides and Isotopes". XVI Edition. KAPL,Inc. 2002
2) "MCNP-A General Monte Carlo N-Particle Transport Code," LA-UR-03-1987, Los Alamos National Laboratory, 2003.
3) D.J. Mitchell, D.R Waymire. "GADRAS User Manual" Sandia National Laboratories. 2009.
4) "PyNE User's Guide" PyNE Development Team. 2011

Results:

Spectra resulting from the counting of irradiated material were created for both the 3 and 14 MeV cases with cooling times ranging from 12 to 72 hours in 12 hour intervals. These spectra were compared at different energies and cooling times. The 14 MeV irradiation consistently showed the production of more activation species. To better quantify the differences in observed gamma ray lines, the ratio of the most intense gamma ray lines were plotted for the 6 observed cooling times. The lines chosen were taken from different activation products to avoid redundant results.

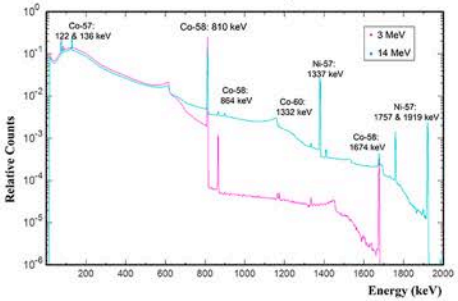

Figure 1: Comparison of Nickel activation spectra irradiated with 3MeV (purple) and 14 MeV (teal) neutrons.

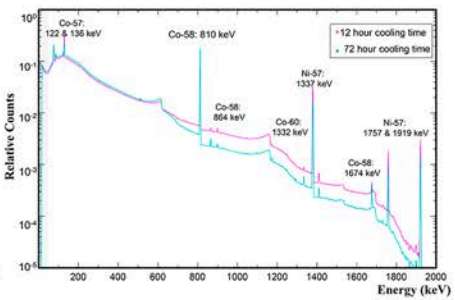

Figure 2: Comparison of 14 MeV Nickel activation spectra with a 12 hour and 72 hour cooling time.

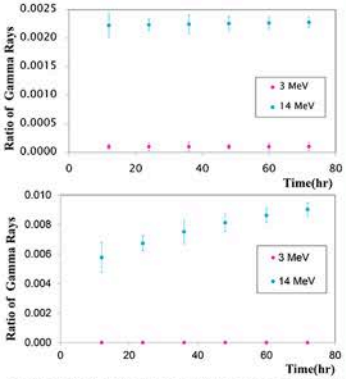

Figure 3 & 4: Ratio of most intense gamma rays over time from 2-3 and 14 MeV irradiation. **Top**: Ratio of Co-57's 122 keV to Co-58's 810 keV. **Bottom**: Ratio of Co-60's 1332 keV to Co-58's 810 keV.

This work was performed under the auspices f the U.S. Department or Energy by Lawrence Livermore National Laboratory under contract No. DE-AC52-07NA-27344

β-Delayed α Angular Correlation in Mass 8 Systems

Richard Beck[1], N. Scielzo[1], Matthew Sternberg[1], P. F. Bertone[3], F. Buchinger[4], S. Caldwell[3,8], A. Chaudhuri[3], J.A. Clark[3], J.E. Crawford[4], C.M. Deibel[5], S. Gulick[4], G. Gwinner[6], D. Lascar[2,3], A.F. Levand[3], G. Li[3,4], G. Savard[3,8], R. Segel[2], K.S. Sharma[6], J. Van Schelt[3,8], R.M. Yee[7], B.J. Zabransky[3]

[1]Lawrence Livermore National Laboratory, [2]Northwestern University, [3]Argonne National Laboratory, [4]McGill University, [5]Michigan State University, [6]University of Manitoba, [7]University of California, Berkeley, [8]University of Chicago

Introduction

THEORY

$$N_{\pm}(\theta, E, E_0) = F(E, E_0)[1 + a_{\pm}(E, E_0)\cos\theta + b_{\pm}(E, E_0)\cos^2\theta]$$

Total spectra | Phase space | Kinematic recoil | Weak interaction

- β-Decay spectrum determined by phase space, kinematic correction, and nuclear structure effects
- Kinematic correction well understood
- Weak interaction term describes the correlation between the direction the beta particle (electron) is emitted and the directions the two alpha particles are emitted

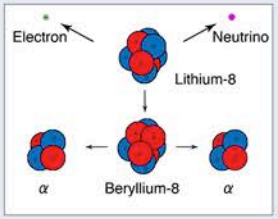

LITHIUM-8

- Lithium-8: isotope of Lithium that has 5 neutrons and 3 protons
- Radioactive, decays into Beryllium-8, which decays into two alpha particles (Helium)
- First β particle emitted, then α particles

Setup

SAMPLE INJECTION

- Lithium-8 is produced using 7Li(d,p) reaction: Lithium-7 beam reacted with Deuterium to form Lithium-8
- Lithium-8 ions stopped, bunched, and purified using Helium gas and electric fields
- Ions held nearly at rest in 1 mm³ volume for accurate measurement using an ion trap.

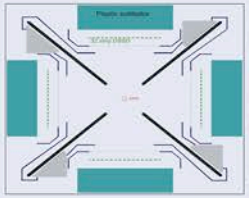

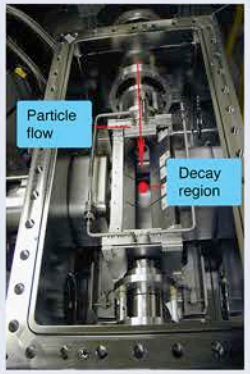

MEASUREMENT

- Detectors: Four 64x64x1 mm³ with 32x32 silicon strips laid perpendicular to each other in front of plastic scintillators
- Measurements give the direction and energy of both alpha and beta particles

Data

SPECTRA

- 3×10⁵ β-α-α coincidences in the decay of Lithium-8 collected with apparatus

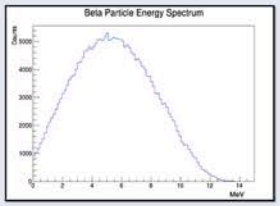

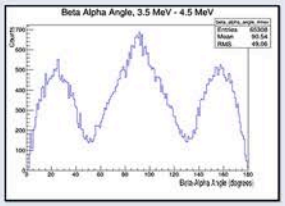

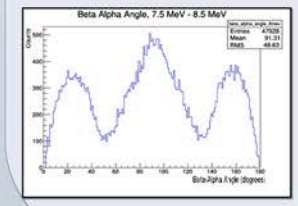

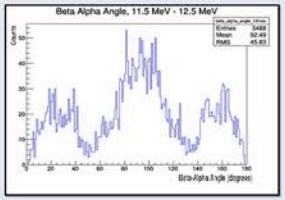

Simulation vs. Observed

SIMULATION

- Simulation reproduces data very well
- Impact of kinematic and weak interaction terms still requires careful comparison
- To interpret data, a simulation of the β decay and the apparatus in GEANT4 physics modeling software was developed to compare to data
- Allows us determination of kinematic and weak interaction terms

UNEXPECTED EFFECT

- As the energy of the beta particle increases, there is some disagreement between data and simulation between 90° and 120°
- Simulation needs reinvestigating and refining in order to uncover source of discrepancy
- Will need to be investigated in Boron-8 data

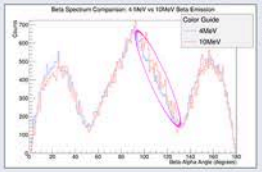

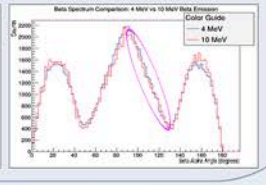

Future Goals

BORON-8 MEASUREMENTS

- Boron-8 data collected, will soon be compared to both simulation and the Lithium-8 data
- Boron-8 has similar decay chain as Lithium-8, except β decay mechanism is positron-emission (β+) instead of electron-emission (β-)
- Mirror decay switches the signs on certain mathematical terms, crucial for isolating the magnitude of said terms
- Will then be able to determine the nuclear recoil terms experimentally
- Require 12.7 million events for 5% uncertainty, and 80 million events for 2% uncertainty.

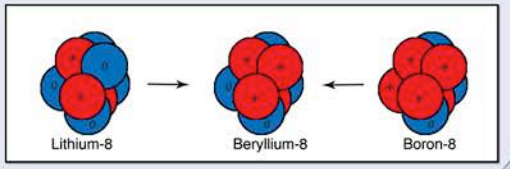

LLNL-POST-658101

This work was performed under the auspices of the U.S. Department of Energy by Lawrence Livermore National Laboratory under contract DE-AC52-07NA27344. Lawrence Livermore National Security, LLC

Lawrence Livermore National Laboratory

Glenn T. Seaborg Institute

Reactor Modeling of Pu and Cs Isotope Ratios in Pressurized Water Reactor Fuel Assemblies

Andrew Conant[1,2], Martin Robel[1], Anna Erickson[1,2]

[1]Lawrence Livermore National Laboratory, Physical and Life Sciences Directorate, Chemical Sciences Division

[2]Georgia Institute of Technology, Department of Nuclear and Radiological Engineering

Georgia Tech

Goal: Model axial variation of $^{240}Pu/^{239}Pu$ and $^{137}Cs/^{135}Cs$ under varying reactor core conditions

Overview:

^{239}Pu is produced in a reactor via the neutron capture of ^{238}U, but some is lost through the fission of ^{239}Pu. ^{240}Pu comes from the neutron capture of ^{239}Pu.

$$^{238}_{92}U + ^{1}_{0}n \longrightarrow ^{239}_{92}U \xrightarrow[23.5\ mins]{} ^{239}_{93}Np \xrightarrow[2.36\ days]{} ^{239}_{94}Pu$$

$$^{239}_{94}Pu + ^{1}_{0}n \longrightarrow ^{240}_{94}Pu$$

^{137}Cs is a fission product with ~6.2% of the cumulative fission yield for the thermal fission of ^{235}U. ^{135}Cs is primarily produced from the decay of ^{135}Xe. However, most of the ^{135}Xe is transmuted to ^{136}Xe ($\sigma = 2.6$ Mb).

$$^{135}_{54}Xe \xrightarrow[9.14\ hours]{} ^{135}_{55}Cs$$

This makes the $^{137}Cs/^{135}Cs$ isotope ratio sensitive to reactor operating conditions.

$$^{235}_{92}U + ^{1}_{0}n \xrightarrow[fissions]{\sim 6.2\%} ^{137}_{55}Cs + other\ fission\ products + ^{1}_{0}n$$

H_20 (light water) and D_20 (heavy water) are used as reactor moderating materials. ^1H and D elastic scattering and absorption cross-sections are shown below.

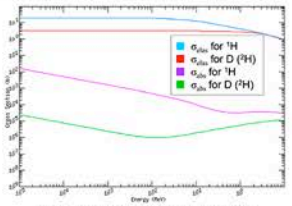

Figure 1: Cross-sections for ^1H and D (^2H) [1]

Method:

mcnp

An infinite-lattice model of the Belgian BR-3 PWR hexagonal fuel assembly (shown below) was made as an input to MCNP6, a Monte Carlo particle transport code. The geometry, composition, and power history of BR-3 assemblies was obtained from INEL[2] and Yamamoto[3]. Isotopics for each burnup step were retrieved from the MCNP output files. Reactor conditions were modified to examine the effects on $^{240}Pu/^{239}Pu$ and $^{137}Cs/^{135}Cs$. Enrichment of the UO_2 fuel and moderator properties are the reactor conditions of interest for this project. These conditions were modified in the MCNP inputs, which were run using the Livermore Computing resources.

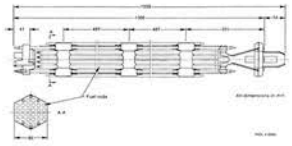

Figure 2: BR-3 Fuel Assembly [2]

Results:

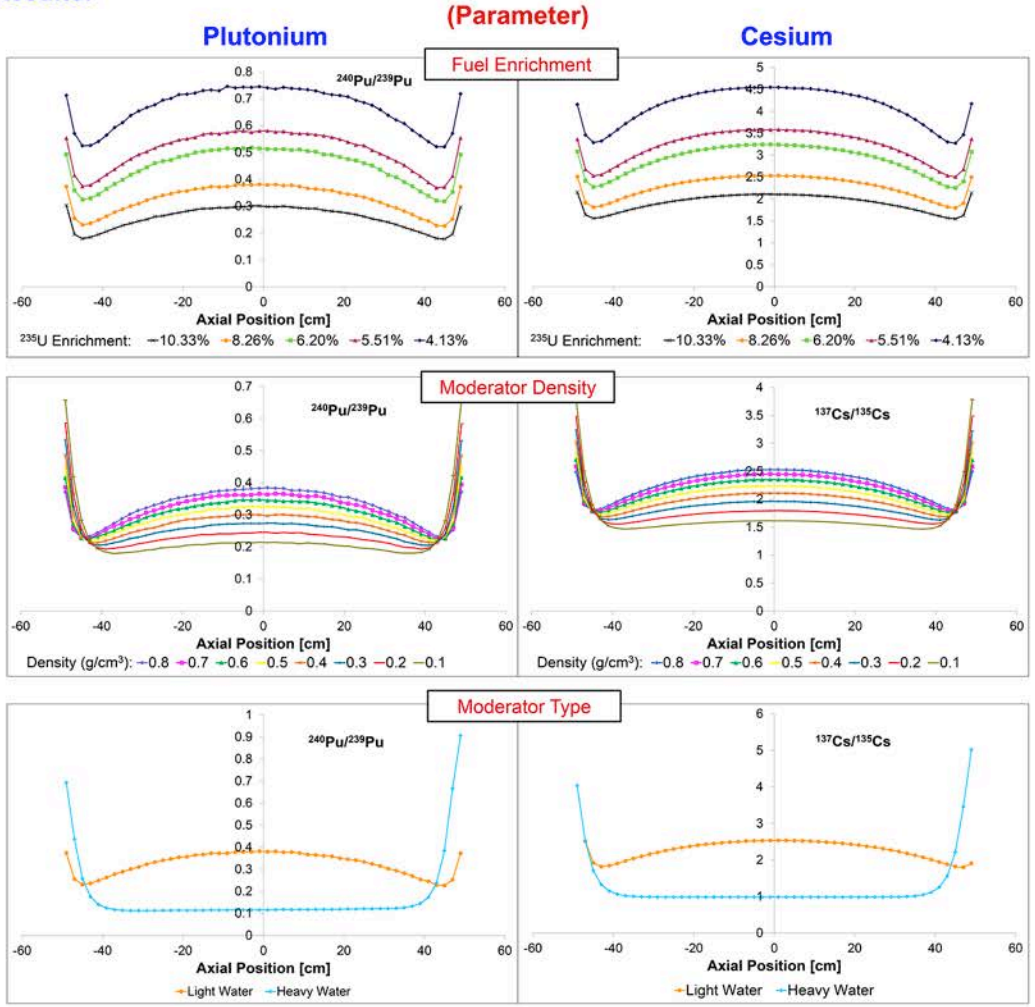

The active fuel length is 100 cm. The axial position of -50 cm is the bottom of the fuel assembly and 50 cm is the top of the assembly. All results are shown for a burnup of 42.26 GWd/MTU.

This work was performed under the auspices of the U.S. Department of Energy by Lawrence Livermore National Laboratory under Contract DE-AC52-07NA27344.
LLNL-POST-658051

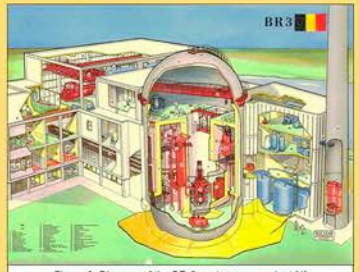

Figure 3: Diagram of the BR-3 nuclear power plant [4]

Conclusion:

$^{240}Pu/^{239}Pu$ and $^{137}Cs/^{135}Cs$ both decrease with increasing enrichment. Increasing the enrichment shifts the neutron spectrum to a higher energy, resulting in more captures of ^{240}Pu.

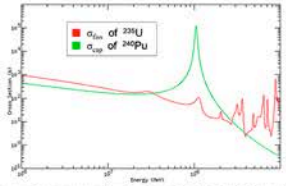

For a given power level, the effect of enrichment on $^{137}Cs/^{135}Cs$ can be explained by:

$$\frac{d}{dt}\left(^{137}_{55}Cs\right) \sim \text{fission rate} \left| \uparrow \frac{^{235}_{92}U}{^{239}_{94}Pu} \right| \downarrow \varphi \left| \uparrow \left[^{135}_{54}Xe\right] \right| \uparrow \frac{d}{dt}\left(^{135}_{55}Cs\right)$$

The flatter distribution of the isotope ratios for the heavy water moderator can be explained by its lower scattering and absorption cross-sections and lower energy transfer per collision. This causes the neutrons to be distributed more evenly.

Future Work:

- Modeling with a deterministic code (e.g. Scale 6.1)
- Test other reactor core and operation conditions (neutron poisons, shutdown length/frequency, core power level, etc.)

References:

[1] Ha, Yeong-Keong et al. "Local Burnup Characteristics of PWR Spent Nuclear Fuels Discharged from Yeonggwang-2 Nuclear Power Plant." Korea Atomic Energy Research Institute.

[2] Adams, James & Burdette, Dabell. "Characteristics of UO_2-Zr Fuel Rods Irradiated in the BR3 Reactor." Idaho National Engineering Laboratory.

[3] Yamamoto, Toru et al. "Analysis of Core Physics Experiments on Fresh and Irradiated BR3 MOX Fuel in REBUS Program." Japan Nuclear Energy Safety Organization.

[4] "Nuclear Reactor Cutaways." BibliOdyssey. Web.

Evaluating Methods for Removing Radioactive Contamination from Traditional Forensic Evidence: Moths

Glenn T. Seaborg Institute

K.A. Daniel[1], R.E. Lindvall[2], L. Richards-Waugh[1], J. Chute[1], and M.J. Kristo[2]

[1]Marshall University Forensic Science Center, 1401 Forensic Science Drive, Huntington, WV 25701
[2]Lawrence Livermore National Laboratory, 7000 East Ave., Livermore, CA 94550

MARSHALL FORENSIC SCIENCE

Goal: Evaluate solvent performance in decontaminating forensic evidence coated in dispersible radioactive material before transitioning into a traditional forensic science laboratory.

Overview:

Two goals of Nuclear Forensics[1]

1. Scientific analysis of nuclear material to determine material properties and origin
2. Traditional forensic analysis of contaminated evidence

Traditional forensic evidence associated with interdicted nuclear material or an attack using a radiological dispersal device (RDD or dirty bomb) may become contaminated by dispersible radioactive material and must either be:

- Analyzed by a laboratory capable of handling dispersible radioactive material
- Decontaminated prior to entering a traditional forensic science laboratory

1 April 2009 – Victoria, Australia[2]

Police carried out a drug raid of an alleged amphetamine laboratory. They unexpectedly found 300 grams of uranium oxide in a storage property. After initial analysis by the Australian Science & Technology Organization (ANSTO), aliquots of the material were sent to Lawrence Livermore National Laboratory (LLNL) for further analysis. While aliquoting the sample for chemical analysis, researchers at LLNL found the body and head of a moth (Figure 1).

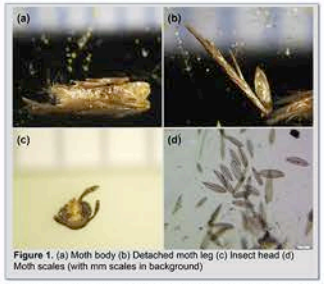

Figure 1. (a) Moth body (b) Detached moth leg (c) Insect head (d) Moth scales (with mm scales in background)

Entomological study of the moth could prove useful for understanding the history of the material from production to interdiction within Australia, a type of signature referred to as a "route attribution" signature in nuclear forensics. However, entomology labs are unequipped to handle dispersible radioactivity.

The decontamination process must remove enough nuclear material to render the evidence safe without destroying the evidentiary value.

Method:

- Exemplar moths were gathered from northern Colorado.
  Pro: readily available, Con: much larger (possibly more durable) than the evidence moth
- CUP-2, an uranium ore concentrate, was used to contaminate the moths.
- Decontamination method: ultrasonication in eleven decontamination solvents (five moths per solvent system).
- Determine decontamination efficacy by mass difference and microscopic examination.

Results:

Microscopic Examination

Two visual indicators of a successful decontamination:

1. Visibly removes the contamination.
2. Does not affect the appearance of the moth.

Figures 2 and 3 demonstrate a partially successful decontamination.

- Figure 2 shows the furry thorax on a moth after contamination. The visible dusty, green particles are CUP-2. After decontamination with water, some small, particles are still visible.

Figure 2. Before decontamination with water.

Figure 3. After decontamination with water.

Figures 4, 5, and 6 demonstrate a completely successful decontamination.

- Figure 4 and 5 show the moth before and after contamination with CUP-2. A solution of 5% Radiacwash™ was used to remove the CUP-2 particles. Figure 6 taken after the decontamination process shows no significant changes to the appearance of the moth.

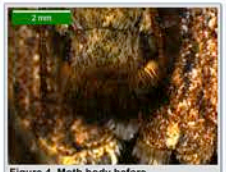

Figure 4. Moth body before contamination.

Figure 5. Moth body after contamination.

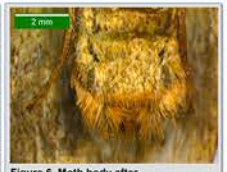

Figure 6. Moth body after decontamination with 5% Radiacwash™.

Figure 7 demonstrates an unsuccessful decontamination.

- The solvent, a solution of 10% RBS™-25 (percentage recommended by the manufacturer), might have left a residue on the moth that resulted in the charred appearance after desiccation at 120 °C. The mass difference data (Table 1) suggests that RBS™-25 could be a viable option; however, the moth lost many body parts (legs, part of a wing, and many scales) that could contribute to the mass loss.

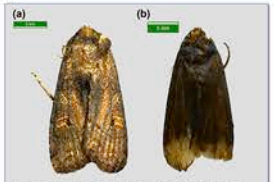

Figure 7. (a) Before and (b) After 10% RBS-25

Results:

Mass difference

The masses of each moth before and after the decontamination process was used to determine the percentage of CUP-2 removed.

Table 1. The mean percentage of CUP-2 removed from the treated moths for each solvent is presented along with the standard error of the mean.

Solvent	Mean % CUP-2 Removed	Standard Error of the Mean
Water	18.7	12.2
3% Citric Acid*	-15.2	15.2
1.4% Sodium Bicarbonate*	62.0	4.6
0.25 M EDTA*	50.2	10.5
1% DTPA*	64.9	13.1
5% Radiacwash™	158.5	32.6
10% RBS™-25	106.7	5.2
5% Decon 90	170.9	50.1
Acetone	147.4	15.5
1% Nitric Acid	119.3	3.9
1M Nitric Acid	99.0	6.6

*Chosen from Ref 3.

Conclusions:

- Solvents found to be qualitatively promising for decontamination include:
  - 5% Radiacwash™, 5% Decon 90, Acetone, and 1% Nitric Acid.
  - These solvents removed the most mass without damaging the moth.
- Mass difference measurements are imprecise due to:
  - Incomplete desiccation – water left in the moth from an incomplete initial desiccation can result in an artificially high mass when compared to the final desiccated mass. An average of 37% of the total body mass was lost during initial desiccation, this may not be a complete desiccation.
  - Loss of body parts during ultrasonication – lost legs and antennae were collected; however, scales were unavoidably lost and might have a significant mass contribution.

Future Steps:

- Complete desiccation of moths for more reliable data – may require the use of isopropanol and/or longer desiccation time with storage in a desiccator.
- Spike samples with known amounts of gamma emitters and determine the amount of decontamination with gamma counting.
- ICP-MS analysis to determine the amount of uranium remaining.
- DNA extraction – can DNA be extracted and separated from the radioactive material for analysis in a traditional forensic science laboratory.

References:

1. Kristo, M. Nuclear Forensics. In: L'Annunziata, MF, editor. Handbook of Radioactivity Analysis. 3rd ed. Oxford: Elsevier, 2012; 1281-1304.
2. Kristo MJ, Keegan E, Colella M, Williams R, Lindvall R, Eppich G, et al. Nuclear Forensic Analysis of Uranium Oxide Powders Interdicted in Victoria, Australia. LLNL-TR-486036.
3. IAEA External and Internal Contamination Decontamination and Decorporation Module XV. http://www.-pub.iaea.org/MTCD/publications/PDF/eprmedt/Day_3/Day_3-12.pps

Acknowledgements:

This work was performed under the auspices of the U.S. Department of Energy by Lawrence Livermore National Laboratory under Contract DE-AC52-07NA27344.

LLNL-POST-658123

Exploring Polymerization Techniques for PSD Plastic Scintillators

Megan E. Deeds, H. Paul Martinez, Andrew Mabe, Leslie Carman, Andrew Glenn, and Natalia Zaitseva*

Lawrence Livermore National Lab, 7000 East Ave. Livermore, CA 94550

University of Cincinnati, 2600 Clifton Ave. Cincinnati, OH 45220

Glenn T. Seaborg Institute

UNIVERSITY OF Cincinnati

Introduction

Neutron detection is important for the detection of nuclear materials. Scintillation techniques have proven to excel in the detection of neutrons for years. Specifically, organic scintillators show promise due to their ability to detect neutrons. Organic scintillators are able to resolve the difference between neutrons and other ionizing particles as well as between neutrons types due to pulse shape discrimination (PSD).

Plastic scintillators have become increasingly attractive due to their robustness. However, compared to both liquid and crystal scintillators, plastics do not perform as well. Performance of scintillators relies heavily on two factors: light yield (LY) and PSD. In order to improve upon these factors, different polymerization techniques have been explored.

PSD Mechanism

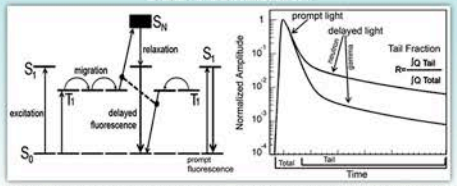

PSD mechanism can be explained via an energy diagram. Excitations due to interactions with differing ionizing particles result in different types of emission, delayed and prompt, which gives rise to the PSD phenomenon. Also included is the initial spectrum of the neutron and gamma waveforms.

Data Analysis

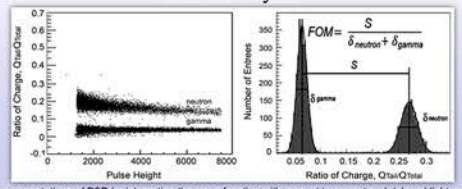

These are representations of PSD by integrating the wave function with respect to prompt and delayed light and using figure of merit (FOM). FOM is determined by taking the separation of the peaks of interest and dividing by the sum of full width at half maximum (FWHM) of the corresponding peaks.

Methods

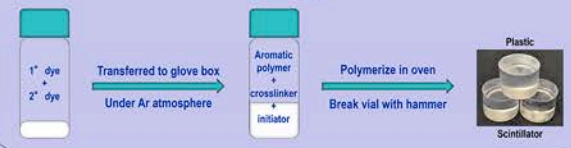

Compounds and Samples

Sample	Sample Description
3941	30%PPO + 5%DVB in PS 10g - Blank
3942	30%PPO + 0.2%NPO + 5%DVB in PS 10g
3943	30%PPO + 0.2%Bis-MSB + 5%DVB in PS 10g
3944	30%PPO + 0.2%Butyl-PBD + 5%DVB in PS 10g
3945	30%PPO + 0.2%Bis-MSB + 5%DVB in PS 10g - No Inhibitor, No Initiator @ 70° C
3946	30%PPO + 0.2%Bis-MSB + 5%DVB in PS 10g - No Inhibitor, w/ Initiator @ 70° C
3947	30%PPO + 0.2%Bis-MSB + 5%DVB in PS 10g - No Inhibitor, No Initiator @ 100° C
3948	30%PPO + 0.2%Bis-MSB + 5%DVB in PS 10g - No Inhibitor, w/ Initiator @ 100° C

Choosing an Effective 2° Dye

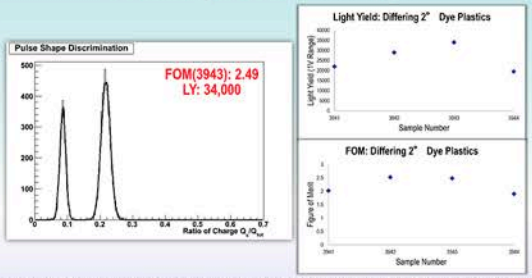

After using multiple secondary dyes, the dye with the greatest light yield and FOM is Bis-MSB. This dye is used as the secondary dye altering the polymerization method.

Polymerizing Under Varying Conditions

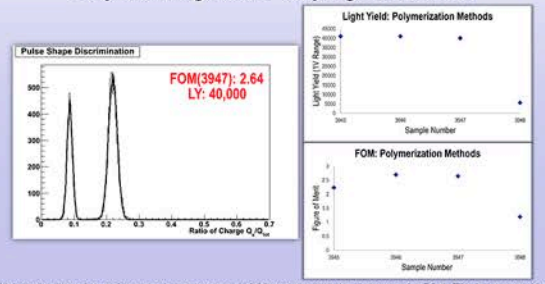

Initial results show that an increase in temperature, in initiator-less samples, improves the FOM. This is not seen in the samples containing initiator, but the sample with initiator at high temperature turned yellow which lowed the LY and the FOM significantly.

Future Work

- Studying additional temperatures will allow for a better understanding of this temperature dependence.

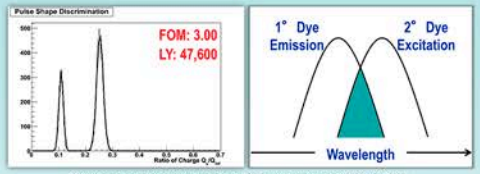

Preliminary results, show that a new 2° dye improves both LY and FOM.

- Use of different dyes and/or initiators that will not yellow in order to increase the light yield and the PSD.

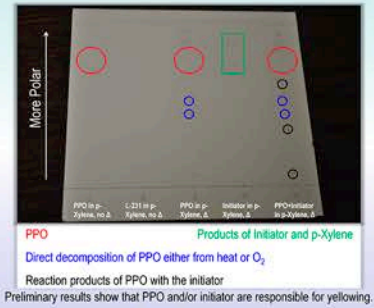

Preliminary results show that PPO and/or initiator are responsible for yellowing.

Conclusions

- Polymerization at higher temperatures show promise in increasing PSD with samples excluding initiator.
- Yellowing of plastics is likely to be PPO and/or initiator. Organics tend to yellow when subjected to heat and naturally overtime due to decomposition of the compound.
- Preliminary results reveal that removal of inhibitor (in styrene) increases LY and PSD. This is possibly due to yellowing and absorbance of light that interferes with efficient energy transfer.

References

[1] J. B. Birks, The Theory and Practice of Scintillation Counting, Pergamon Press, London, 1964.

[2] N. Zaitseva, A. Glenn, L. Carman, R. Hatarik, S. Hamel, M. Faust, B. Schabes, N. Cherepy, and S. Payne, "Pulse Shape Discrimination in Impure and Mixed Single-Crystal Organic Scintillators," *IEEE Transactions on Nuclear Science*, vol. 58, no. 6, pp. 3411-3420, 2011.

[3] N. Zaitseva, B. L. Rupert, I. Pawelczak, A. Glenn, H. P. Martinez, L. Carman, M. Faust, N. Cherepy, and S. Payne, "Plastic scintillators with efficient neutron/gamma pulse shape discrimination," *Nuclear Instruments and Methods in Physics Research A*, vol. 668, pp. 88-93, 2012.

Lawrence Livermore National Laboratory

LLNL-POST-658086

This work was supported by the U.S. DOE, NNSA, Office of Defense Nuclear Nonproliferation, Office of Nonproliferation Research and Development (NA-22)

This work performed under the auspices of the U.S. Department of Energy by Lawrence Livermore National Laboratory under Contract DE-AC52-07NA27344

Understanding Plutonium in Fallout Formation

Fitzgerald, Marc[1]; Knight, Kim[2]; Ramon, Erick[2]; Czerwinski, Ken[1]; Hutcheon, Ian[2]

1. University of Nevada Las Vegas
2. Lawrence Livermore National Laboratory

Glenn T. Seaborg Institute

Soil composition is the fundamental parameter controlling plutonium incorporation in fallout

Abstract

Fig 1: Nuclear fallout originates from soil swept into the fireball during the nuclear explosion. Figure A is an image of soil found near Trinity ground zero. This soil is swept up by the fireball, represented by image B, where it is subject to thermodynamic conditions that result in the formation of aerodynamic fallout, image C.

Recent analyses have shown Trinity fallout to be compositionally heterogeneous glassy material reflecting a mixture of local soil and bomb debris. This compositional diversity provides a wealth of previously overlooked information, including phase-composition, diffusive-convective mixing/transport, and phase-activity associations. My work characterizes heterogeneity in major element chemistry and Pu distribution to understand how the composition of the local environment, represented by soil, affects partitioning of plutonium during fallout formation. Analytical measurements were made using SEM-EDS and autoradiography. Pu / major element correlation was understood through principal component analysis. Results show that Pu is correlated with Fe and Ca. These results, augmented by theoretical and experimental work, will inform a model capturing the first-order effects responsible for compositional heterogeneities in fallout.

Analytical Approach

Goal: To understand Pu correlation with major elements

- Ten aerodynamic glasses from Trinity were selected for analysis
  - Polished to expose the spherule midsection
- Major element composition characterized using Energy Dispersive X-ray Spectroscopy (SEM-EDS)
  - Quantitative spatial mapping of Al, Ca, Fe, Na, Mg, Si, and K
- Autoradiography was used to characterize relative Pu concentrations
  - Autoradiography signal intensity is proportional to Pu concentration

Primer: Principal Component Analysis

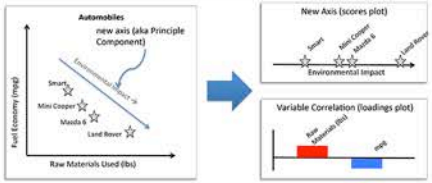

Fig 2: Principal Component Analysis (PCA). PCA is a data reduction technique that seeks to reduce complex multidimensional datasets into two or three dimensions. In the example above, the basis is fuel economy and raw material. PCA redefines the basis with respect to the variance in the dataset (Environmental Impact). This transforms a two dimensional dataset into a one dimensional dataset. A PCA solution includes variable weightings, which can be used to understand correlation or anticorrelation between variables.

Numerical Approach

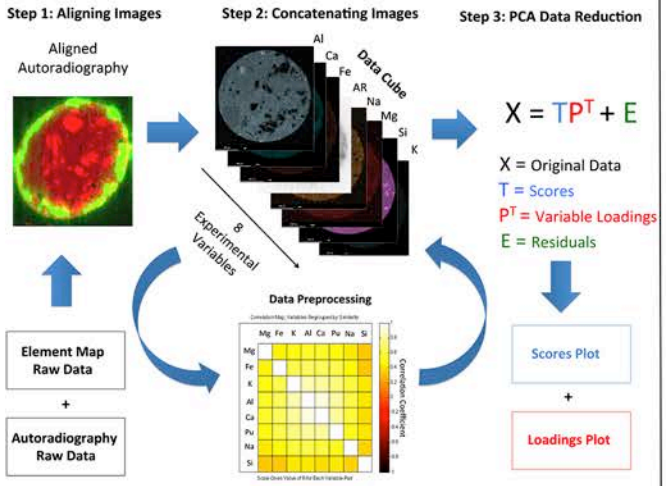

Fig 3: Numerical approach to data reduction is performed in three steps:

1. Autoradiography data are aligned with and scaled to the resolution of the EDS image.
2. Data are concatenated into a 3 dimensional array. The array is transformed into a correlation matrix by mean centering variables followed by scaling by the unit variance.
3. Data array is reduced using PCA, producing a score and loadings plot.

Results and Discussion

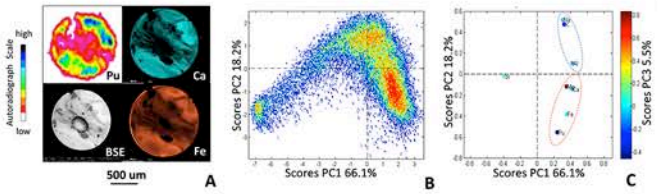

Fig 4 A, B, & C: Sample T12. Panel A shows an autoradiography image, a backscattered electron image representing compositional heterogeneity, and EDS maps for Ca and Fe. For EDS maps, areas of higher intensity correspond to elevated Ca and Fe. Pu appears correlated with Ca and Fe rich regions. Panel B shows PCA scores from the combined data cube of EDS and autoradiograpy data. Areas of sparse data are represented by blue while areas of data clustering are represented by red. Regions where data cluster reflect primary compositions present in the fallout, and tend to correlate well with major rock-forming mineral compositions. Panel C shows PCA variable loadings suggesting compositional relationships in the fallout. In the example of T12, a positive correlation of Pu, Ca, and Fe, reflective of the correlations observed in panel A, is evident.

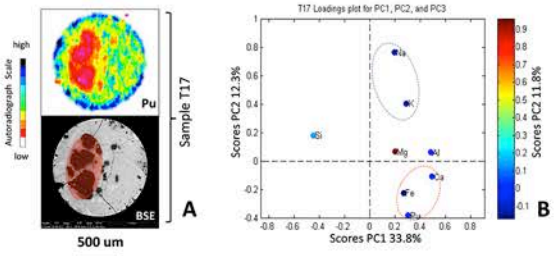

Fig 5. A & B: PCA Data reduction of sample T17. In this sample, correlation between Pu and major elements is unclear based on visual examination of EDS maps (not shown). Exclusion of low activity regions identified by autoradiography, indicated by red shading on the BSE image (panel A) permits examination of-Pu and major element variance within the regions of the sample clearly retaining device signatures. The PCA loadings plot, panel B, shows that Pu concentrations, where present, are strongly correlated with Fe and Ca.

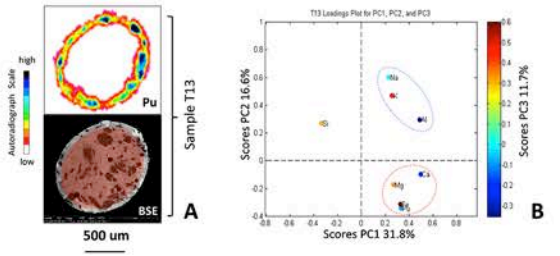

Fig 6. A & B: PCA Data reduction of sample T13. Like sample T17, spatial relationships between Pu distributions and major elements in sample T13 EDS data are not apparent through visual inspection, alone. A targeted approach, excluding regions of low to no activity, reveals correlations between Pu, Ca, Fe, and Mg, and anti-correlations with K and Na, as observed in samples T12 and T17.

Conclusion

- PCA analysis of compositional data for T12, T13, and T17 shows correlations between Pu, Fe, and Ca in all three samples.
- Correlation in multiple samples from the same event suggests a common chemical and physical environment
  - May reflect the refractory nature of Pu, Ca, and Fe
  - May reflect the viscosity and surface tension of the molten precursor
- **Future Work: Targeted approaches using spatially resolved isotopic and concentration measurements of Pu in combination with modeling will be used to understand observations**

References

1.) Smith, Lindsay. A tutorial on Principal Component Analysis. http://mx-www.informatik.uni-bremen.de/664/1/smith_tr_02.pdf (Accessed Aug-1-2014)

This research was performed under the Nuclear Forensics Graduate Fellowship Program, which is sponsored by the U.S. Department of Homeland Security, Domestic Nuclear Detection Office. This work was also performed under the auspices of the U.S. Department of Energy by Lawrence Livermore National Laboratory under Contract DE-ACS2-07NA27344, including financial support from the U.S. Department of Energy's National Nuclear Security Administration, Office of Defense Nuclear Nonproliferation Research and Development.
LLNL-POST-658049

Local and Global Nuclear Fallout Contributions to a Soil Profile

Connor Hilton[1,2], Ross Williams[2], Richard Bibby[2], Theresa Kayzar[2], Kerri Schorzman[2]
[1]Brown University, Department of Earth, Environmental, and Planetary Sciences
[2]Chemical Sciences Division, Glenn T. Seaborg Institute, Lawrence Livermore National Laboratory

Purpose: Investigate the movement of Pu, U, and Cs deposited from atmospheric weapons testing in a soil profile (0-16 cm) from Currant Summit Spring (CSS), NV

Background:

- At the Nevada National Security Site (formerly Nevada Test Site), 97 atmospheric nuclear tests were conducted from 1951-58 and 3 in 1962[1]
- Most NNSS fallout trajectories went east but some went northeast, over CSS[2]
- The Limited Test Ban Treaty in 1963 banned further atmospheric testing in the US[1]
- Over 500 atmospheric tests have been conducted around the world from 1945 until 1980[3]

Methods:

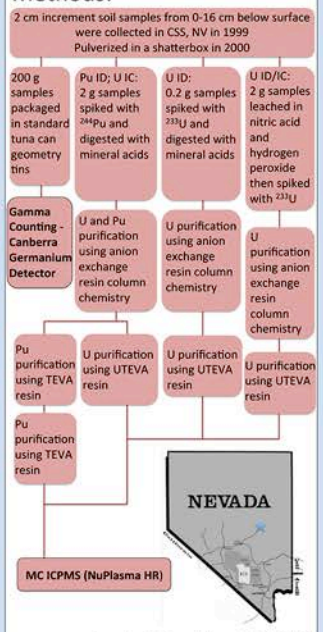

Sample site in relation to the NNSS[4]

Results:

Pu

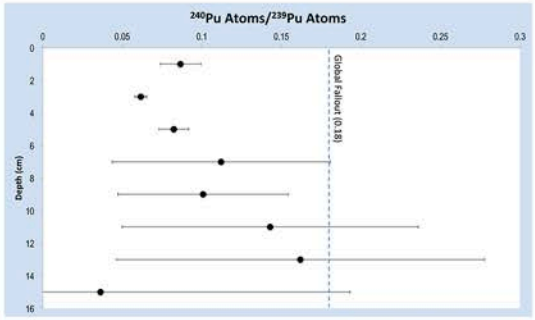

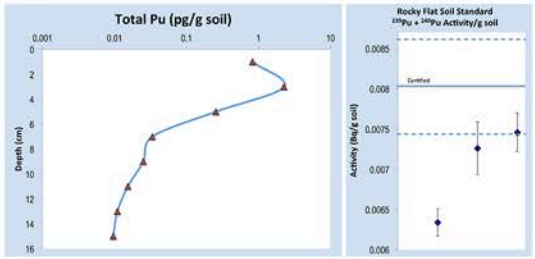

- Noticeable NNSS contribution causing a lower Pu ratio than the accepted global fallout level of 0.18[5]

U

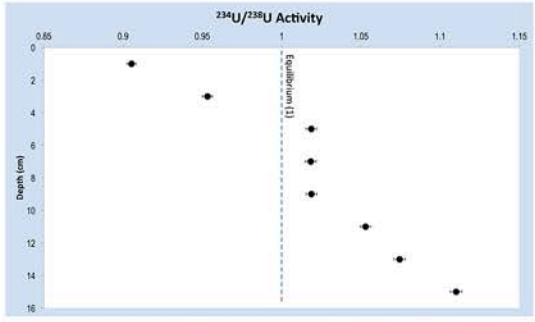

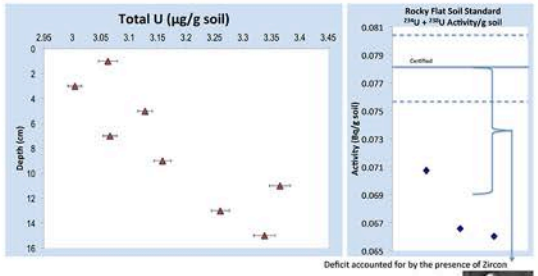

- Activity ratios suggest leaching of natural ^{234}U from the upper soil and transport into the deeper soil[6]

Cs

- ^{137}Cs fallout from weapons testing is concentrated in the upper 4 cm of soil

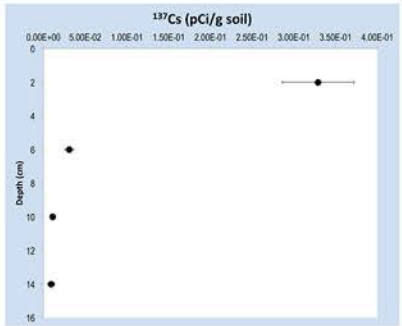

236U

- Mineral acid digestion yielded higher ^{236}U concentrations than selective leaching

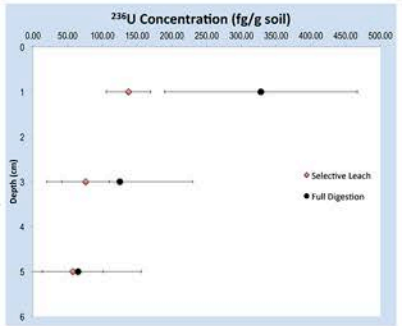

Conclusions:

- Noticeable atmospheric weapons testing fallout contribution to the top 6 cm layers shown by $^{240}Pu/^{239}Pu$, ^{137}Cs and ^{236}U
- Noticeable NNSS weapons testing fallout contribution to the top 6 cm layers shown by $^{240}Pu/^{239}Pu$
- Evident leaching of ^{234}U into deeper soil, possibly by water infiltration
- Total U concentrations within the range of accepted average levels in soils (≈3 ppm)[7]

Further Work:

- Repeat Pu analyses to determine reproducibility of the data
- Account for the RFS standard Pu deficit
- Collect 8 new CSS soil samples to measure isotopic signature changes after 15 years
- Determine how U is bound in the soil through more systematic leaches

Citations:

[1]The History of the Nevada Test Site and Nuclear Testing Background. *National Cancer Institute, National Institute of Health* [Online], 2.1-2.24.
[2]Miller, Richard. *Under the Cloud: The Decades of Nuclear Testing*. London: Collier Macmillan Publishers, 1986.
[3]Turner, Mary; et al. Excess plutonium in soil near the Nevada Test Site, USA. *Elsevier* [Online], 2003, 125, 193-203. http://dx.doi.org/10.1016/S0269-7491(03)00071-X.
[4]Fehner, Terrence R.; Gosling, F. G. Origins of the Nevada Test Site. *United States Department of Energy* [Online], 2000. DOE/MA-0518.
[5]Williams, R. W.; et al. Local and Global Fallout Preserved in Lake Sediment from the Sierra Nevada, California. APSORC '09 [Online], 2009. LLNL-ABS-415241.
[6]Kayzar, Theresa M.; et al. Investigating uranium distribution in surface sediments and waters: a case study of contamination from the Juniper Uranium Mine, Stanislaus National Forest, CA. Journal of Environmental Radioactivity [Online], 2014, 136, 85-97. http://dx.doi.org/10.1016/j.jenvrad.2014.04.018.
[7]Uranium Fact Sheet. Health Physics Society, Specialists in Radiation Safety. 2011.

This work was performed under the auspices of the U.S. Department of Energy by Lawrence Livermore National Laboratory under Contract DE-AC52-07NA27344.

LLNL-POST-657803

Relative Sensitivity Factors for Manganese and Chromium in Minerals Measured by Secondary Ion Mass Spectrometry (SIMS)

Christine E. Jilly[1,2], Benjamin Jacobsen[1], Jennifer Matzel[1], Ian D. Hutcheon[1], Patricia Doyle[2]

[1]Lawrence Livermore National Laboratory, Livermore CA, 94550. [2]University of Hawai'i at Mānoa, HIGP, Honolulu HI, 96822.

Motivation

The ^{53}Mn-^{53}Cr radiochronometer is useful for dating aqueous alteration events in chondrites [1]. Secondary minerals (e.g., carbonates, fayalite) can be measured in situ using SIMS. However, to obtain accurate ages, the Mn/Cr relative sensitivity factors (RSFs) must be determined for the mineral being measured. Historically, San Carlos olivine has been used as a proxy for fayalite and carbonate RSF, but recent measurements [e.g. 2] have shown that small compositional changes can have a large impact on the RSF.

► **We address this problem by analyzing a variety of Mn and Cr enriched minerals to determine how mineral composition affects the RSF, and to observe shifts in the Mn-Cr isochron due to changes in RSF.**

The relative sensitivity factor:

$$RSF = \frac{(^{55}Mn^+/^{52}Cr^+)_{SIMS}}{(^{55}Mn/^{52}Cr)_{TRUE}}$$

Varies with:
- Mineral composition
- Instrumental tuning
- Duration of measurement

Samples

- Carbonates (e.g., calcite, dolomite) and fayalite are common secondary minerals in chondrites used for Mn-Cr radiometric dating.
- Mn- and Cr-bearing carbonates and fayalite are not naturally occurring on Earth, difficult to obtain adequate SIMS standards.
- We analyzed synthetic Mn- and Cr- bearing calcite [2] and fayalite crystals [3], as well as silicates and carbonates implanted with Mn and Cr ions.

Figure 1: *Optical images of some Mn-, Cr-bearing standards measured here. From left: Synthetic calcites mounted in bullet from [2], ion-implanted fayalite, ion-implanted carbonate minerals mounted in epoxy plug, provided by J. Matzel.*

Analytical Methods

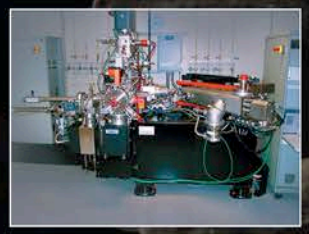

NanoSIMS:
- Hyperion O source
- Spot size: 5 x 5 µm raster
- Ions measured: $^{55}Mn^+$, $^{52}Cr^+$, $^{44}Ca^+$, $^{30}Si^+$, $^{25}Mg^+$
- Mass resolving power: ~4500
- True value determined by EPMA
- Data reduction using L'Image and Excel software

Figure 2: *NanoSIMS at Lawrence Livermore National Laboratory.*

Results and Discussion

Ion implant samples:
- Observed Gaussian distribution of implanted Mn^+ and Cr^+ with depth (Fig. 3)
- Homogeneous lateral distribution of Mn^+ and Cr^+ in conductive samples.
- Insulating samples (e.g. carbonates) were poorly implanted (Fig. 3 inset), likely due to charge build-up during the implantation process.
- RSFs to be determined after SIMS pits are analyzed with a profilometer, and EPMA.

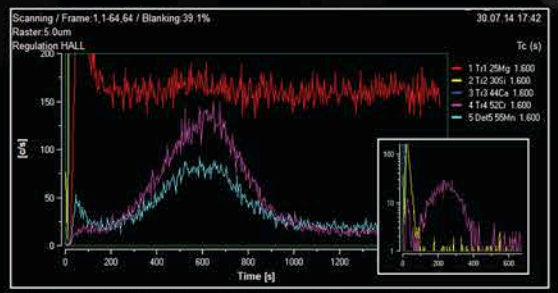

Figure 3: *Example of a Gaussian implant profile of Mn^+ and Cr^+ ions into conductive substrate, in this case a Si-wafer. Graph displays ion counts per second versus measurement time.* ***Inset:*** *Characteristic implant profile for Cr^+ into carbonate minerals.*

Synthesized minerals:

RSF values were determined for three samples (Fig. 4).

Figure 4: *Relative sensitivity factors for measured minerals. The average values are denoted by the dashed lines: approx. 1.6 for synthetic fayalite, 1.1 for a Mn,Cr pyroxene glass, and 0.8 for synthetic calcite.*

An isochron with initial ratio of $(^{53}Mn/^{55}Mn)_0 = 3.42\times10^{-6}$ would yield a formation age of ~3.6 Myr after CAI formation if not corrected for RSF.

RSF-corrected ages:
- RSF 1.6 → 1.2 Myr
- RSF 1.1 → 3.2 Myr
- RSF 0.8 → 4.8 Myr

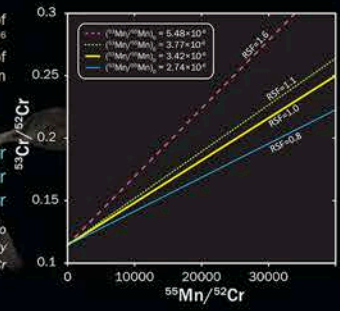

Figure 5: *Sample isochrons to show how RSFs from this study would affect the slope of a Mn-Cr measurement (data from [4]).*

Conclusions

► **Improper RSFs can shift the Mn-Cr isochron leading to dating errors up to ~4 Myr; therefore, proper matrix-matched standards must be used.**

► **Work in progress: future work includes using a profilometer to determine the penetration depth of the Mn^+ and Cr^+ in implanted standards. New carbonate implants to be made using a faraday cage to prevent charging.**

References: [1] Shukolyukov A. and Lugmair G. (2006) *Earth Planet. Sci. Let.* 250, 200-213. [2] Sugiura N. et al. (2010) *Geochem. J.* 44, e11-e16. [3] Doyle P.M. et al. (2013) *LPSC XLIV*, #1719. [4] Jilly C. E. et al. (2014) *Meteorit. Planet. Sci.*, doi: 10.1111/maps.12305

High-Energy Neutron Foil Activation for Davis Cals

Corey Keith[1], Tomi Akindele[2] Bryan Bandong[3], Robert Haslett[3], Tzu Wang[3], Kevin Roberts[3]

[1]Texas A&M University, Department of Nuclear Engineering, College Station, TX

[2]University of California, Berkley, Department of Nuclear Engineering, Berkley, CA

[3]Lawrence Livermore National Laboratory, Physical and Life Sciences Directorate, Chemical Sciences Division, Livermore CA

Davis Cals are inter-laboratory measurements and calibration comparisons of "threshold detector products". High-energy neutron foil activation is used for the radioisotope production, and the goal is to model this process and compare to experimental results.

Introduction

Radioanalytical measurements on activation products are conducted by LLNL, LANL, PNNL and UK's AWE as part of an inter-laboratory calibration study. The activation species are produced at the 76-inch Cyclotron at UC Davis Crocker Nuclear Laboratory by irradiating various metal foils with spallation neutrons from a Be target bombarded with deuterons. The activation species produced will vary based on experimental parameters (such as beam energy and Be target thickness), and these effects were evaluated. Because the existing data for (d,n) reactions in beryllium, as well as production cross sections for the foils, are limited in the evaluated energy ranges, we investigated the use of a combination of experimental data and physics models utilizing MCNPX.

Neutron Flux Profile/Depth

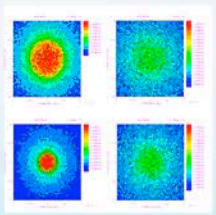

The neutron flux profile on Al foil with Be thickness of 0.1, 0.3, 0.5, and 0.7 cm starting from bottom left clockwise respectively.

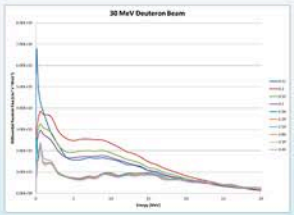

The differential neutron flux for different Be thickness with a 30 MeV deuteron beam.

Setup

The various physics models used to model (d,n) reactions incorporated both INC and Evaporation physics. Scoping work showed that for 40-MeV deuterons, changes in evaporation models had little impact and so the Bertini[2] model was used. MCNPX2.7 was used to evaluate neutron transport in the system and reaction rates in the foils. The model of the beryllium target and foil system is shown below.

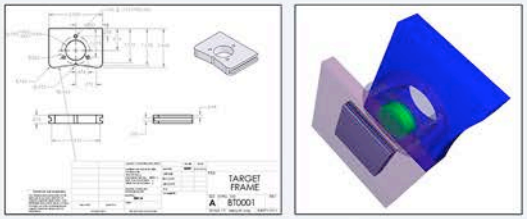

The schematics and MCNP modeled beryllium target and foil apparatus.

Neutron Flux

The production pathways in various foils will have high energy dependence. The resulting neutron energy flux from deuteron bombardment will influence what isotopes are favorably produced and in what ratios.

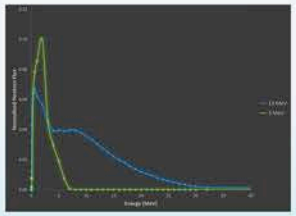

The normalized neutron flux at 28 MeV and 6 MeV deuteron beam incident on a Be target.

Activation Species Production

Activation species production for 10 foils (Al, Ti, Fe, Ni, Cu, Ir, W, Pt, Au, and Pb were evaluated at two different deuteron beam energies. Various neutron capture reactions were considered for production, such as (n,d), (n,t), (n,3n) etc. The results for Ti and Ni foils for the 28 MeV deuteron beam are presented below.

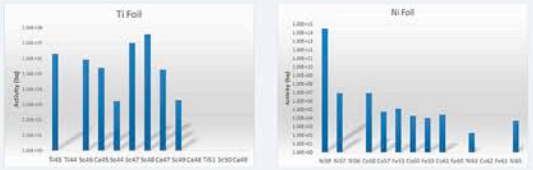

The modeled isotopics produced in Ti and Ni foil in units of activity. ENDF cross-sections were used to calculate the production

Discussion

Scoping studies were done to evaluate different beryllium thicknesses for a given deuteron beam energy. This was used to guide the design of the target for optimum neutron yield, minimized thermalization, and improved beam geometry. The isotope production in foil will be energy dependent, with the many production pathways having varying thresholds. Depending on the target nuclide(s) that is desired to be produced, different energy regimes will be needed.

References:

1. S.G. Mashnik, et al., LANL Report LA-UR-05-7321, Los Alamos, 2005, RSICC Code Package PSR-532, http://www-rsicc.ornl.gov/codes/psr/psr5/psr532.htm.
2. H.W. Bertini Phys. Rev., 131 (1963), p. 1801
3. A. Boudard *et al.* Phys. Rev. C, 66 (2002), p. 044615

This work performed under the auspices of the U.S. Department of Energy by Lawrence Livermore National Laboratory under Contract DE-AC52-07NA27344.

LLNL-POST-658159

SIMS Analysis of Aerodynamic Fallout

Characterizing the distribution of residual fuel in glassy aerodynamic fallout from a uranium-fueled test

Laurence A. Lewis[1,2], K.B. Knight[2], W. Kinman[3], J.E. Matzel[2], S.G. Prussin[1], F.J. Ryerson[2], M.M. Zimmer[3], I.D. Hutcheon[2]

[1]Department of Nuclear Engineering, University of California, Berkeley
[2]Chemical Sciences Division, Glenn T. Seaborg Institute, Lawrence Livermore National Laboratory
[3]Nuclear and Radiochemistry Group, Los Alamos National Laboratory

Glenn T. Seaborg Institute

The distribution of residual fuel in 5 aerodynamic fallout glasses was determined using secondary ion mass spectrometry (SIMS) and correlated with bulk features in the glasses using scanning electron microscopy (SEM) and electron probe microanalysis (EPMA).

Overview

Glassy fallout forms when a nuclear device is detonated near the Earth's surface. Soil is melted and vaporized and swept up into the fireball, where it interacts with device debris. As molten fallout leaves the fireball, drag forces create a variety of aerodynamically-shaped fallout glasses.

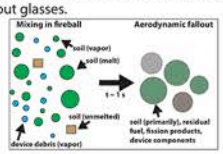

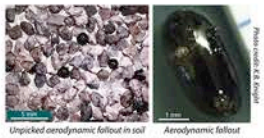

Unpicked aerodynamic fallout in soil — Aerodynamic fallout

Photo credit: K.B. Knight

Aerodynamic fallout has been shown to host the majority of the radioactivity and contain elevated concentrations of residual fuel, compared to other types of fallout (Eppich et al, 2014). However, how that fuel distributes itself within individual fallout glasses is poorly understood and may provide information on how device debris interacted with the environment to form fallout. **Therefore, spatially-resolved analyses within single samples can possibly elucidate fallout formation mechanisms, temperatures, and timescales.**

Samples

Samples are both compositionally heterogeneous and homogeneous

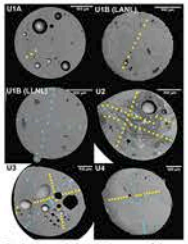

Backscattered electron images of the samples with SIMS analysis locations marked. Blue circles: LLNL; Yellow squares: LANL

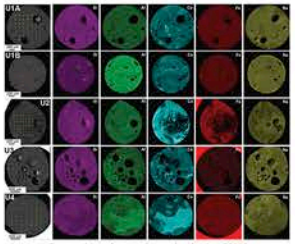

Compositional maps determined using EPMA

All samples show mixing and flow. U2 and U4 show evidence for molten agglomeration of distinct molten silicates, followed by rapid cooling.

Representative aerodynamic fallout

Currently, five samples have been analyzed. However, there are plans to analyze over 30 additional aerodynamic fallout glasses.

Secondary Ion Mass Spectrometry (SIMS)

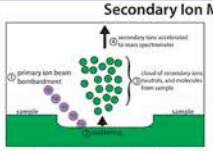

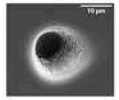

Spatially-resolved (~10 µm), high-sensitivity (~1 ppm) isotopic measurements

Results

A range of U isotopic ratios was measured within the samples, spanning nearly three orders of magnitude in $^{235}U/^{238}U$, indicating significant uranium isotopic heterogeneity both between samples and within individual samples (Eppich et al., 2014). **Between all five samples, the $^{235}U/^{238}U$ ratio spans a factor of greater than 500, from 0.02 to 11.8. Within a single sample, U2, the $^{235}U/^{238}U$ ratio ranges from 0.02 to 7.81, a factor of nearly 400.**

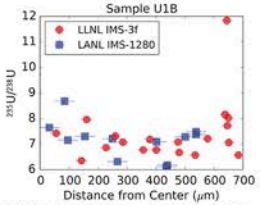

$^{235}U/^{238}U$ as a function of distance from the center of the sample for U1A

While the samples display a large range of $^{235}U/^{238}U$ ratios, sample U1A is homogeneous with respect to both chemical composition and uranium isotope ratios, except for the $^{235}U/^{238}U$ ratio of 11.8 measured near the periphery of U1B. **To achieve this degree of homogeneity, these samples may have been held above the melting temperature long enough for the combined effects of mixing and diffusion to effectively homogenize the melts prior to quenching.**

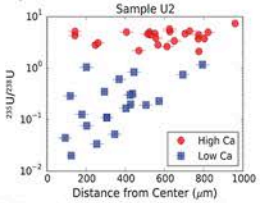

$^{235}U/^{238}U$ as a function of distance from the center of the sample for U2, segregated by measurements made in high and low Ca regions of the sample.

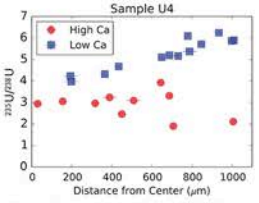

$^{235}U/^{238}U$ as a function of distance from the center of the sample for U4, segregated by measurements made in high and low Ca regions of the sample.

Samples U2 and U4 display correlations between the $^{235}U/^{238}U$ ratios with composition, specifically Ca. In U2, two distinct components are evident: one with $1 < {}^{235}U/^{238}U < 8$, which is associated with the brighter contrast regions in the backscattered electron image (CaO ~1.5 wt.%), and the other with $0.02 < {}^{235}U/^{238}U < 1$, which is associated with the darker contrast regions (CaO ~ 0.5 wt.%). The $^{235}U/^{238}U$ ratio in sample U4 also displays a bimodal isotopic behavior, but exhibits the opposite correlation between the $^{235}U/^{238}U$ ratio and Ca concentration. Regions enriched in ^{235}U are depleted in Ca (CaO ~2 wt.%), while regions depleted in ^{235}U are enriched in Ca (CaO ~3.5 wt.%). **These correlations suggest that these glasses incorporated different amounts of unfissioned fuel from the device, and then cooled too quickly to fully homogenize.**

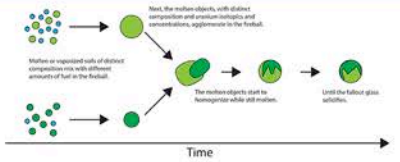

Likely formation steps for U2 and U4

The observations in samples U2 and U4 suggest that silicates formed by swept up soil becoming molten and interacting with device debris before colliding with other molten silicate droplets of different chemical and U-isotope composition in the debris cloud, and finally solidifying. The time scale for cooling of such melts is predicted (Glasstone and Dolan, 1977; Izrael, 2002) and observed (Cassata et al., 2014) to be on the order of seconds.

Mixing Model

This variation in the $^{235}U/^{238}U$ ratio provides evidence for the inclusion of at least two components with different uranium isotopic compositions in fallout: one enriched in ^{235}U from the device, and the other reflecting natural isotopic composition uranium derived from soil and/or the device. We can then construct a simple model based on the mixing of two, isotopically distinct end-members. For this model we assume the fuel has a $^{235}U/^{238}U$ ratio of oralloy, or ~ 17.3 (Moody, 1994), and natural composition $^{235}U/^{238}U$ is 0.0072.

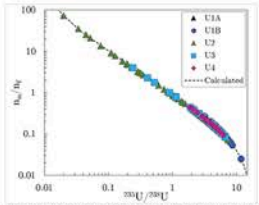

Contributions of uranium of natural composition (n_n) relative to uranium from the enriched end-member (n_f) as a function of the $^{235}U/^{238}U$ ratio for all samples. The dashed line represents depicts the shape of the mixing line. The mixing line asymptotically approaches infinity as the $^{235}U/^{238}U$ ratio approaches the composition of natural uranium, $^{235}U/^{238}U = 0.0072$, and asymptotically approaches zero as the $^{235}U/^{238}U$ ratio approaches 17.3, the $^{235}U/^{238}U$ ratio in oralloy (Moody, 1994).

Future Work

- Examine correlations between $^{235}U/^{238}U$ and fallout size
- Examine correlations between $^{235}U/^{238}U$ and distance of collection
- Quantitate relationship between $^{235}U/^{238}U$ and composition

References

-Cassata, W. S., Prussin, S. G., Knight, K. B., Hutcheon, I. D., Isselhardt, B. H., & Renne, P. R. (2014). When the dust settles: stable xenon isotope constraints on the formation of nuclear fallout. Journal of Environmental Radioactivity, 137, 88-95.
-Eppich, G. R., Knight, K. B., Jacomb-Hood, T. W., Spriggs, G. D., & Hutcheon, I. D. (2014). Constraints on fallout melt glass formation from a near-surface nuclear test. Journal of Radioanalytical and Nuclear Chemistry, 1-17.
-Glasstone, S., & Dolan, P. J. (1977). The effects of nuclear weapons. In The effects of nuclear weapons. US Department of Defense; US Department of Energy.
-Izrael, Y. A. (2002). Radioactive fallout after nuclear explosions and accidents. Elsevier.
-Moody, K. J. (1994). Dissolved oralloy standards and the origin of HEU. No. UCRL-ID-117611. Lawrence Livermore National Lab., Livermore, CA (United States).

This work performed under the auspices of the U.S. Department of Energy by Lawrence Livermore National Laboratory under Contract DE-AC52-07NA27344. We thank the U.S. Department of Energy's National Nuclear Security Administration, Office of Defense Nuclear Nonproliferation Research and Development for financial support.

LLNL-POST-658080

Investigation of Radium Analytical Methods for Groundwater with Complex Matrices

Andrew M. Renshaw*+, Richard K. Bibby+, Stephanie H. Uriostegui+, Gary R. Eppich+, Jean E. Moran*, & Bradley K. Esser+

*California State University, East Bay, Hayward, California, 94542, United States

+Lawrence Livermore National Laboratory, Livermore, California, 94550, United States

Introduction

California's diverse geology is reflected in a wide range of groundwater chemical composition. Understanding the hydrogeology and geochemistry of California's ambient groundwaters is important for identifying the impact of conventional or unconventional oil & gas development on groundwater quality. One potential impact is radioactivity. Flowback and produced waters from hydraulic fracturing operations in Pennsylvania are high in radium (up to 17,000 pCi/L; Nelson et al., 2014). Flowback and produced waters are also saline, and Nelson et al. (2014) have shown that EPA protocols for the determination of radium in drinking water underestimate Ra activity in high-salinity produced waters. In order to accurately and efficiently analyze Ra in such groundwater, we are modifying current protocols for use with high-salinity groundwater.

Matrix Complications

Produced and formation waters associated with hydraulic fracturing are difficult to analyze using clean water methods. Co-precipitating Ra out of solution is inefficient due to high concentrations of other constituents. The adjacent table shows the concentrations of major ions in flowback fluid from the Marcellus Shale in Pennsylvania (Nelson et al., 2014).

Analyte	Concentration (mg/L)
Chloride	146,667
Strontium	36,333
Sodium	29,333
Calcium	13,000
Barium	9,000
TDS	277,666

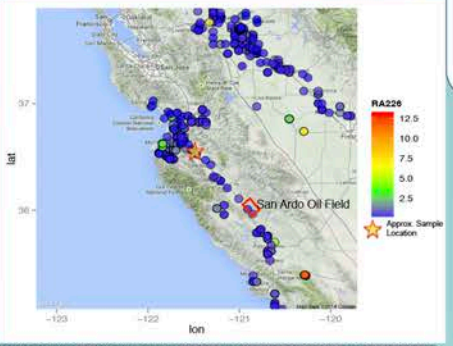

Radium-226 activity (pCi/L) in drinking water production wells from portions of the Salinas Valley and San Joaquin Valley. Data obtained from the USGS and California SWRCB GAMA database. The San Ardo Oil Field is highlighted in red.

Experimental Approach

- Analyze the applicability of Liquid Scintillation Counting (LSC) for rapid and robust quantification of alpha emitting radium isotopes, mainly ^{226}Ra.
- Establish a minimum detectable activity (MDA) using standards and samples of known activity.
- Compare and complement LSC data with RAD7 radon detector and HPGe Gamma Spectroscopy data analysis.
- Analyze groundwater samples from the Salinas Valley utilizing LSC and the RAD7.

Methods

1. QUANTULUS Liquid Scintillation Spectrometer:
   - Samples placed in LSC vial with 10mL sample overlain by 10mL mineral cocktail. Counted for between 30 and 60 minutes for multiple cycles.
2. DURRIDGE Co. RAD7:
   - The RAD H_2O accessory for the RAD7 was utilized to analyze hermetically sealed 250mL Salinas Valley samples and a laboratory prepared ^{226}Ra standard.
3. HPGe Gamma Spectroscopy:
   - LSC vials with known ^{226}Ra and natural U activities were counted for 1200 minutes. Samples sit 33mm from the face of the detector. Efficiency values are generated through LabSocs software.

LSC Vial Geometry

The LSC vial analyte is 10mL of sample overlain by 10mL of mineral cocktail. ^{226}Ra decay products (^{222}Rn, ^{218}Po, ^{214}Po, ^{214}Pb and ^{214}Bi) partition into the mineral cocktail, which acts as a scintillant. LSC detects the alpha emission of ^{222}Rn, ^{218}Po and ^{214}Po. The HPGe Gamma Spec counts either gamma emitted by ^{226}Ra in the sample or by ^{214}Pb and ^{214}Bi in the cocktail, depending on analytical configuration.

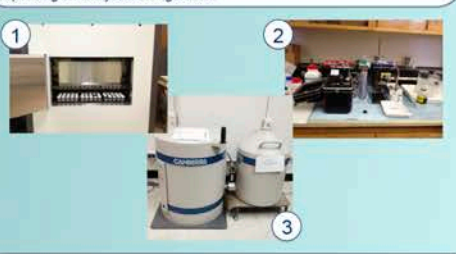

Methods of ^{226}Ra analysis in groundwater. 1) Quantulus Liquid Scintillation Counter 2) Durridge RAD7 3) High-Purity Germanium (HPGe) Gamma Spectroscopy

Discussion

1. LSC (Quantulus):
- No sample prep; high efficiency; small sample volume (10mL).
- MDA: 4.7-8.7 pCi/L
- Recovery is insensitive (<5% difference) to sample/cocktail ratio.
- Recovery not affected by uranium concentration.
- Can rapidly process large number of samples.

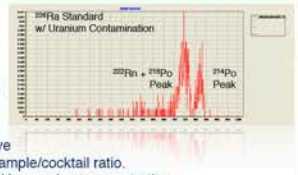

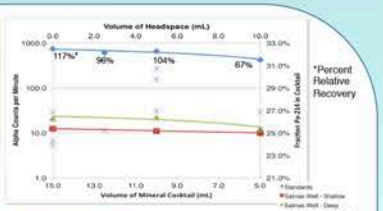

2. Radon detector (RAD7)
- Salinas Valley groundwater has higher activities of ^{226}Ra than the Salinas River
- RAD7 ^{226}Ra is systematically lower than LSC ^{226}Ra.

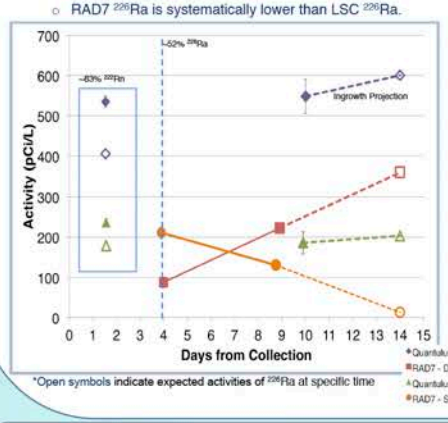

3. HPGe Gamma Spec

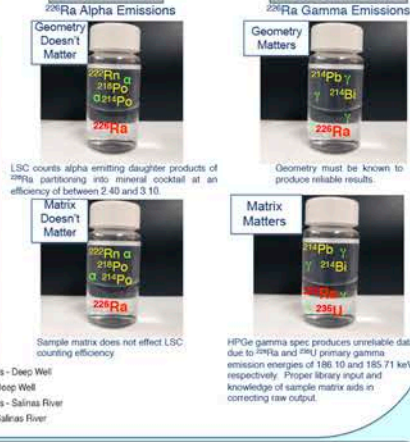

Conclusions

- LSC is a robust and efficient method for quantifying ^{226}Ra in groundwater.
- ^{226}Ra MDA and recovery is not affected by the presence of uranium or by cocktail/sample mixing ratio.
- RAD7 systematically underestimates ^{226}Ra activity, most likely due to loss of ^{222}Rn in the sampling process.
- HPGe gamma spectrometry is accurate with little to no sample prep, but requires strict attention to analytical parameters.
- HPGe gamma spec may be a good QA/QC for LSC.

Future Work

- Fabricate a synthetic sample that resembles flowback or formation water from a hydraulic fracturing operation, and compare the performance of the three methods in high-salinity matrices.
- Further define regional differences in the radium activity in ambient groundwater in California in order to establish background (mean activity and variability).

Glenn T. Seaborg Institute

Lawrence Livermore National Laboratory

This work was performed under the auspices of the U.S. Department of Energy by Lawrence Livermore National Laboratory under Contract DE-AC52-07NA27344. IM Release # LLNL-POST-657988

Lawrence Livermore National Laboratory

Glenn T. Seaborg Institute

Comparison of historical fallout with representative soil samples by XRD and ICP-MS

Rodrigo N. Tapia, Sarah Roberts, Gary Eppich, K. B. Knight, I. D. Hutcheon

The University of Georgia

Goal: to understand relationships between soil mineral phases and chemical composition in the fallout formation process

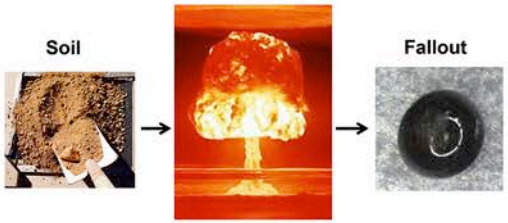

Overview:

We hypothesize that the chemical composition of nearby surface soils will, to a large extent, define the chemical composition of fallout formed during near-surface nuclear tests. In order to better understand the relationship between soil and fallout, several analyses were performed.

•The mineralogical composition of **the soil samples** were determined quantitatively by X-ray diffraction, using the data reduction software TOPAS.

•**Fallout samples**, of subequal diameter (~1.3 mm) and mass 2170 – 4607 μg, were dissolved using mineral acids, and analyzed by quadrupole inductively coupled plasma mass spectrometry (Q-ICPMS), and isotope dilution mass spectrometry (IDMS) using a multicollector-ICPMS (MC-ICPMS) for chemical and uranium isotopic composition.

Fallout Chemical Composition

Major Elements in Fallout Samples

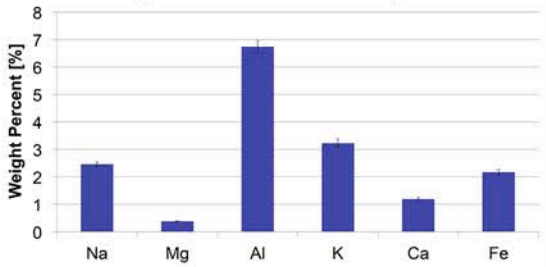

Average weight % of major elements in fallout with average diameter ~1.3 mm, measured by Q-ICPMS. Silicon and oxygen were not measured, but are assumed by difference to constitute ~75 wt. % of the sample.

Results: X-ray Diffraction of Soils

Soil samples representative of those that formed the fallout were ground to micron size particles and analyzed by x-ray diffraction on Bruker D8 X-ray diffractometer. Samples were scanned from 5 – 75° 2Θ. Mineral phases were identified using DIFFRAC.EVA software and powder diffraction file database.

Qualitative Phase Identification

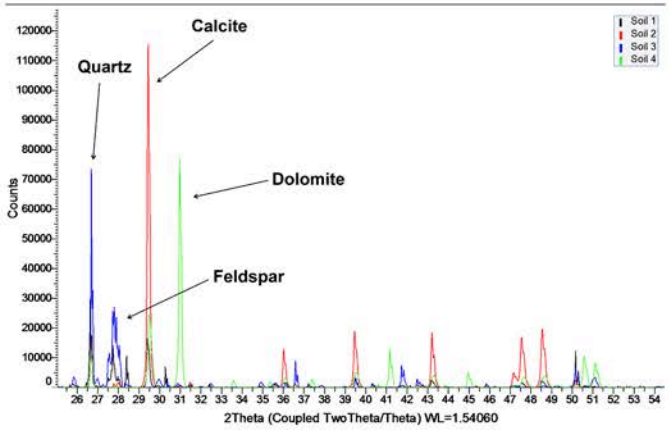

Quantitative Mineral Data of Soils

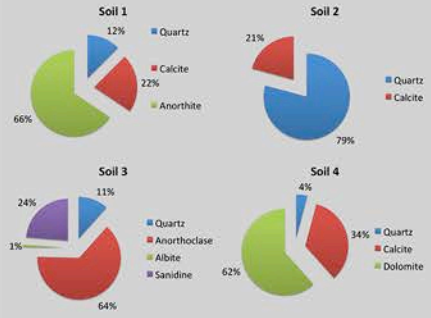

XRD spectra were analyzed quantitatively using TOPAS software. ~20% of NIST LaB_6 was added to each sample for use as an internal standard.

These soils are representative of some of the different types found near ground zero. In order to improve comparisons between fallout and soil compositions, a sample dominated by more quartz and feldspar phases will be studied next.

Results: Fallout Sample Analyses

Fallout sample compositions are compared to those previously studied of a larger size fraction (~1.85 mm diameter, Eppich *et al.*, 2014, *J. Radioanal. Nucl. Ch.*). K_2O variation is 18% of total K_2O composition.

wt% difference between size fractions

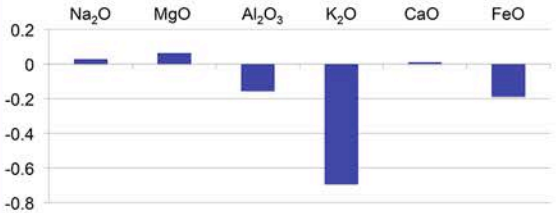

Fallout Uranium Isotopics

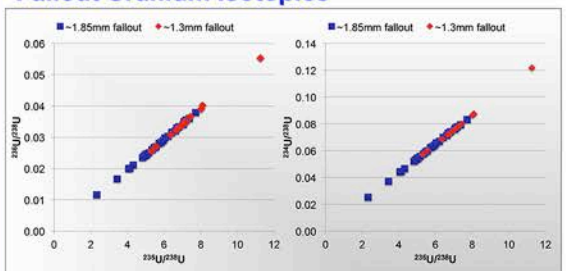

Uranium isotope ratios of fallout samples of two size fractions measured by isotope dilution using MC-ICPMS, with U concentration compared to a larger size fraction. All of these ratios increase with increasing U concentration. Uncertainties are smaller than symbols.

	Avg. U conc. (μg/g)	surface area/volume (mm^{-1})
~1.3 mm Size Fraction	30.798	0.577
~1.85 mm Size Fraction	23.629	0.405
% Difference	*26.3%*	*34.9%*

Conclusions:

- Chemical and mineral compositions may define characteristics such as melting point and viscosity which could greatly influence fallout formation
- Fallout U isotopic composition is suggestive of two-component mixing between naturally-occurring U in soil and highly-enriched, device-derived U
- The smaller size fraction is significantly (26%) more concentrated in uranium, similar to the difference in surface/volume ratio (35%), which suggests that device-derived uranium may be concentrated on the surface of fallout.

This work performed under the auspices of the U.S. Department of Energy by Lawrence Livermore National Laboratory under Contract DE-AC52-07NA27344. We thank the U.S. Department of Energy's National Nuclear Security Administration, Office of Defense Nuclear Nonproliferation Research and Development, for financial support. LLNL-POST-458076